Onset of smoldering and transition to flaming fire

Bjarne Christian Hagen

Dissertation for the degree of Philosophiae Doctor (PhD)

Department of Physics and Technology
University of Bergen

April 2013

Scientific environment

The Ph.D candidate has followed the doctoral training and Ph.D-courses at the Department of Physics and Technology at the University of Bergen (UiB). Associate Professor Bjørn J. Arntzen (UiB) has been the main Advisor and Professor Vidar Frette (Stord Haugesund University College) has been Co-Advisor.

The Ph.D candidate has been employed at Stord Haugesund University College (Høgskolen Stord/Haugesund) while working on the Ph.D. The work presented in this thesis has been completed in full at Stord Haugesund University College. Stord Haugesund University College has also funded the work through grants, funding of equipment and salary.

Acknowledgements

I would like to thank my advisor Associate Professor Bjørn J. Arntzen for accepting me into the Ph.D.-studies at the University of Bergen (UiB) and Stord Haugesund University College (HSH), for making it possible for me to undertake a Ph.D-study.

At HSH I have had two advisors: Professor Vidar Frette and Assistant Professor Gisle Kleppe. Without their help, encouragement and critical feedback, I would not have succeeded in my studies. I cannot thank you enough! I would also thank the former Fire Chief in Bergen Trygve Conradi for advising me to start studying fire safety and my professors at the University of Maryland for sparking the interest for fire research. A special thanks to Prof. James A. Milke for pointing at smoldering fire as an interesting field of research. My thanks also extend to my colleagues Associate Professor Bjarne P. Husted and Assistant Professor Arjen Kraaijeveld at HSH for all their help and encouragement, and to Professor Emeritus Rolf Eckhoff for interesting lectures at UiB. I would like to thank the following for help during preparation of the cotton samples used: D.P. Agnew, M. Arranz, T.G. Hagen, H. Janitz, B. Krause and D.S. Young.

I also have a wonderful and supporting family: my wife Anne Mari and children Tor Gunnar, Ole Christian, Henning and Sofie. They have supported me and reminded me of other important things in life: Pizza on Fridays, trips to Denmark, happy summer holidays and long breakfasts on Saturday mornings. I would also thank my parents: Anne-Berit and Gunnar Hagen for their encouragement and support.

Thank you!

Bjarne Christian Hagen
Haugesund April 2013

Abstract

Aim: The aim of this work has been to investigate the effects of density, heat flux and boundary conditions on smoldering. Two focus areas were chosen: the onset of smoldering and the transition from smoldering to flaming fire.

Methods: Experiments using cotton batting were chosen to study smoldering combustion. Cotton was chosen since it can easily be compressed to a range of densities. Cotton, being mainly cellulose, is a material prone to smoldering.

The cotton was compacted to a predetermined density and heated from below using a hotplate. Five densities were investigated: 20, 40, 60, 80 and 100 kg/m^3, with six heat flux scenarios and two sets of boundary conditions.

Findings: Results from paper I and II show that density affects the onset of smoldering. Samples with high density had lower ignition temperature than samples with lower densities. The temperature for onset of smoldering was reduced from 318 °C to 303 °C as the density of cotton was increased from 40 to 100 kg/m^3. Here, the cotton was heated with high heat flux for 15 minutes and then the hotplate was switched off (Scenario A).

In paper II it is shown that heat flux has an impact on the onset of smoldering, but not on the smoldering process as such. A low constant heat flux for 4 to 5 hours leads to ignition at 284 °C (Scenario D), while a high heat flux for 15 minutes gives 303 °C (Scenario A). Samples exposed to a continuous low constant heat flux have lower onset temperature than samples exposed to high heat flux for a short time.

In paper III two boundary conditions were tested with four densities: 20, 60, 80 and 100 kg/m^3. A solid boundary (a wall) along one of the vertical sample sides leads to reduced smoldering velocity locally, probably as a result of more restricted oxygen transport into the sample. Smoldering velocities that differ spatially make it possible for smoldering and secondary char oxidation to coexist in the sample. The smoldering produces gaseous fuel and the secondary char oxidation ignites the gas, leading to flaming combustion.

Conclusion: Density affects the onset of smoldering, the smoldering combustion and the transition from smoldering to flaming. The heat flux scenario affects the onset of smoldering, but not the smoldering process. The boundary affects the spatial propagation of smoldering in a sample, and through it the transition from smoldering to flaming fire.

Keywords: Smoldering, transition to flaming, ignition, onset of smoldering, density, heat flux scenario, boundary condition.

List of Papers

1. B. C. Hagen, V. Frette, G. Kleppe, B.J. Arntzen, *Onset of Smoldering in Cotton: Effects of Density*, Fire Safety Journal, Volume 46, Issue 3, April 2011, Pages 73-80

2. B. C. Hagen, V. Frette, G. Kleppe, B.J. Arntzen, *Effects of Heat Flux Scenarios on Smoldering in Cotton*
   Submitted to Fire Safety Journal

3. B. C. Hagen, V. Frette, G. Kleppe, B.J. Arntzen, *Transition from Smoldering to Flaming Fire in Small Cotton Samples with Asymmetrical Boundary Conditions*
   Draft, to be published

Contents

List of Figures

Nomenclature

Symbol	Description	Unit
A	area	m^2
A^*	pre-exponential factor	s^{-1}
b	negative slope of the linear temperature profile	$K\ m^{-1}$
Bi	Biot number	[-]
C	concentration	$mol\ m^{-3}$
C_p	specific heat	$J\ kg^{-1}\ K^{-1}$
E_a	activation energy	$J\ mol^{-1}$
ΔH_c	heat of combustion	$J\ kg^{-1}$
h	convective heat transfer coefficient	$W\ m^{-2}K^{-1}$
k	thermal conductivity	$Wm^{-1}K^{-1}$
l	characteristic length	m
l_R	reaction layer thickness	m
$\dot{q}''$	heat flux pr. area	$W\ m^{-2}$
$\dot{q}'''$	heat production pr. volume	$W\ m^{-3}$
R	universal gas constant	$J\ K^{-1}mol^{-1}$
r_0	characteristic length	m
t	time	s
T	sample temperature	K
$T(z)$	sample temperature at height z	K
T_a	ambient temperature	K
T_{lim}	limiting sample temperature	K
T_P	the hotplate temperature	K
T_m^P	Temperature at mode m at time step p	K
V	volume of the sample	m^3
W	mass of cotton	kg
z	height within cotton	m
Δz	distance between nodes	m

Symbol	Description	Unit
α	thermal diffusivity	m^2/s
β	material dependent constant	$s\ m^{-2}$
δ	heat production	[-]
ε	porosity	[-]
κ	permeability	m^2
ρ	density	kg/m^{-3}
$\Delta\tau$	time step	s

Chapter 1

Introduction

Smoldering fire is an interesting combustion phenomenon that gone undetected may cause fire, explosions and death. In spite of this hazard, smoldering is still not fully understood by the fire safety community.

1.1 Problem statement

Smoldering fires represent a hazard both in homes and industry. Due to its slow combustion, smoldering is difficult to detect with ordinary smoke detectors [19]. If a smoldering fire goes undetected, it represents a hazard for occupants in a building. In Norway, 5 % of the fires in dwellings result from smoldering fires, 22 % of the fire deaths in USA are caused by smoldering, while figures from Germany show that 11 % of dust explosions are caused by deep-seated smoldering fires [2, 26, 30].

1.2 Project motivation

A substantial amount of work has been done on smoldering fires. Reviews by Babrauskas [10], Ohlemiller [61] and Rein [72] display the complexity of smoldering fire. One of the less understood aspects is the transition from smoldering to flaming fire. Transition from smoldering to flaming fire has been reported by different researchers, but has not been studied systematically. Smoldering, on the other hand, has been thoroughly reported [59, 79]. Since the transition from smoldering to flaming is a concern for domestic fires, woodland fires, aeronautics and spaceflight [72], a better understanding of the mechanisms causing the transition is desirable.

Earlier works show that density affects smoldering. Lawson found that cellulose insulation resistant to onset of smoldering at low densities, ignites and smolders at higher densities, i.e

when packed more tightly [10, 44]. Ohlemiller and Rogers found that the ignition temperature for cellulose insulation decreased around 10 °C with a 50 % increase in density [55, 64]; while Chan and Napier reported a decrease in the ignition temperature of cotton from 350 to 220 °C as the density increased from 6 to 36 kg/m^3 [20]. Furthermore, Lawson, Wakelyn and Hughs report that if materials such as cotton and cellulose are sufficiently densely packed, there will be no ignition of deep-seated smoldering fires [44, 84].

In the present work, possible effects of density variations for the onset of smoldering and for the transition from smoldering to flaming fires will be investigated. Transition from smoldering to flaming fire has been observed previously for experiments where the smoldering combustion front met a solid boundary [59]. Possible effects of variations in sample density in connection with a solid boundary (a wall) and the transition from smoldering to flaming fire will be considered in the present study.

1.3 Scope and limitations

The scope of this work is to investigate the effects of density on the onset of smoldering and on the transition from smoldering to flaming fire. The onset of smoldering will be approached using different modes of heating. The transition to flaming will be investigated using samples with small heights (0.15 m) in order to isolate possible effects of boundary conditions.

1.4 Clarification of terms

Smoldering is a slow, low-temperature, flameless form of combustion. The combustion is self-sustained due to heat generated by an exotherm reaction between oxygen and solid fuel [62]. The term smoldering is often used interchangeable with other terms. A short discussion of some terms follows to avoid misunderstandings.

A material will thermally decompose when exposed to heat. If the degradation occurs without the presence of oxygen, the process is defined as pyrolysis. Combustion is the degradation of the material in the presences of oxygen [62, 65]. The pyrolysis is an endoterm reaction, while combustion is an exotherm reaction [65].

Smoldering and glowing fire are words that are often used as interchangeable. However, there are differences. Glowing fires combust solid materials without the presence of a flame, but with emittance of light. Smoldering fires, however, combust solid materials without emittance of light [1]. If a smoldering fire reaches high enough temperatures, the materials will begin to glow and the combustion will be referred to as a glowing fire [10].

Glowing fires can also occur as a result of external heat sources such as thermal radiation.

The thermal radiation heats the material to a temperature where it begins to glow [10].

Chapter 2

Previous research

Research on ignition and combustion is documented as far back as the Romans [18], while smoldering combustion came into focus in the 1940s [10]. This chapter gives a short review of previous work on smoldering.

2.1 Fundamentals of smoldering fires

Smoldering fire is a slow, low-temperature, flameless form of combustion. The combustion is sustained by the heat generated by the exothermic reaction between oxygen and solid fuel [62]. Only porous materials forming a solid carbonaceous char when heated, have been found to undergo smoldering combustion [24]. Some of the materials that are prone to smoldering are [10]: wood, cotton, paper, leather, forest duff, coal, charcoal, cigarettes eta.

2.1.1 Qualitative description of smoldering

A smoldering fire will develop three different zones in the sample that is combusted. In figure 2.1, the three zones and unburnt fuel are illustrated [52, 65].

Degradation zone: The degradation zone is characterized by temperature rise, evaporation of water, outflow of visible gases and smoke, and discoloration of the material. In this zone there can be either an endothermic degradation of the fuel (pyrolysis) or an exothermic oxidation degradation of the fuel, depending on the availability of oxygen [65].

Smoldering reaction zone: The reaction zone is characterized by a maximum temperature due to the smoldering combustion of the fuel. There are no visible gases, however, glowing may occur [24]. The fuel is degraded material and char. The char may at a later stage be combusted in what is called secondary char oxidation [68].

Ash: A zone consisting of very porous char and ash which cools off slowly and no longer

glows [24].

Figure 2.1 illustrates a smoldering scenario where the heat is generated in the reaction zone due to combustion of degraded material and char. The heat is transported into the degradation zone where it causes the material to discolor and degrade. The degradation of the material produces gases that can be observed as smoke above the sample. As the material is consumed, ash is produced, forming the last zone [24].

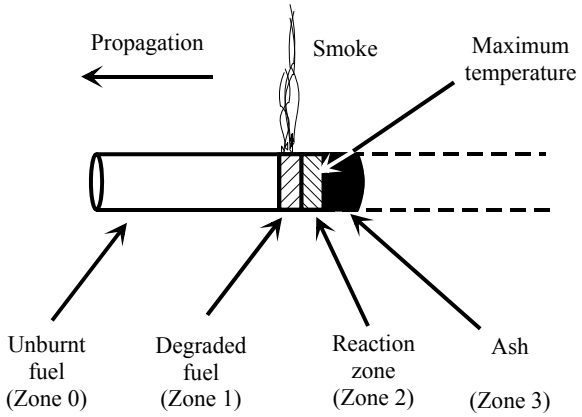

Figure 2.1: Schematic description of smoldering, following Moussa [52] and Drysdale [24]. The four zones discussed in the text are shown, together with the direction of propagation.

2.1.2 Propagation of smoldering fires

When a smoldering fire consumes a sample, air in motion inside and around the sample will affect the propagation of the fire. This leads to a complex three-dimensional combustion process. To scrutinize the mechanisms at work, smoldering has been studied in simplified situations, with quasi-one-dimensional geometry. This is typically achieved using long, narrow samples and forced air from one direction [10]. Two different propagation systems are commonly used (see figure 2.2) [24, 62]:

- Forward smoldering: the air moves in the same direction as the smoldering front.
- Reverse smoldering: the air moves in the opposite direction of the smoldering front.

Forward and reverse smoldering are suitable concepts for describing one-dimensional combustion systems as illustrated in figures 2.1 and 2.3. The simplification gives an important insight

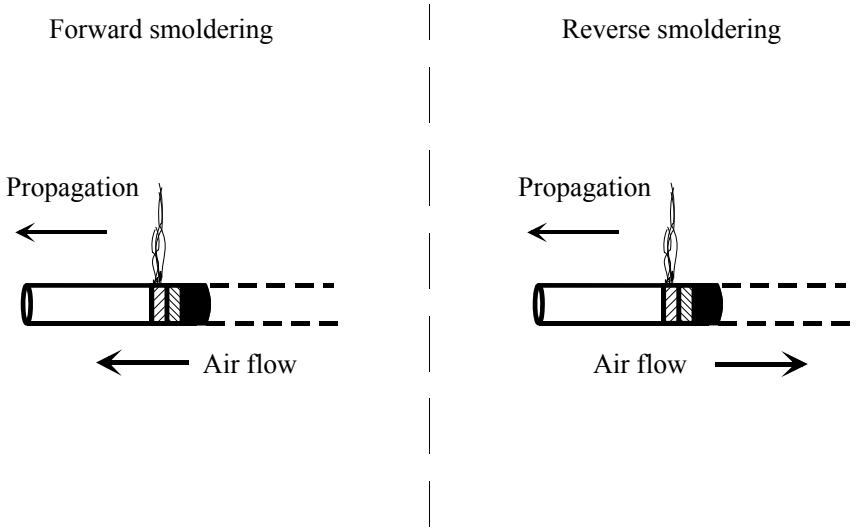

Figure 2.2: Forward and reverse smoldering [63, 71]. The smoldering propagation is related to the direction of air flow with air flow, respectively, in the same and opposite direction as compared to the smoldering propagation.

into the different combustion and heating regimes, and how oxygen affects both the smoldering rate and the combustion products. However, researchers caution against using one-dimensional data in three-dimensional situations, due to the lack of research on three-dimensional systems [10].

Forward smoldering

In a forward smoldering fire, the air moves in the same direction as the smoldering reaction zone [57]. As a result, the oxygen moves through the ash to reach the smoldering reaction zone (see figure 2.3a). The reaction zone consists of partially decomposed fuel and un-oxidized char that will oxidize when in contact with oxygen. The oxidation of the fuel will continue until all the fuel is consumed [14, 62].

The consumption of all oxygen in the reaction zone will affect both the smoldering propagation and the mode of combustion. Heat and combustion products generated in the reaction zone, are transported to the degradation zone, contributing to the heating of the fuel [10]. In forward smoldering, the oxygen enters the smoldering reaction zone through the ash. As the oxygen moves through the reaction zone, it is consumed. Thus, the reaction zone can only move forward when the char does not consume all oxygen, but some of the oxygen reaches the front of the zone [62]. Since most of the oxygen is consumed in the reaction zone, the fuel typically pyrolyses in the degradation zone [62]. Only combustion products and heat will

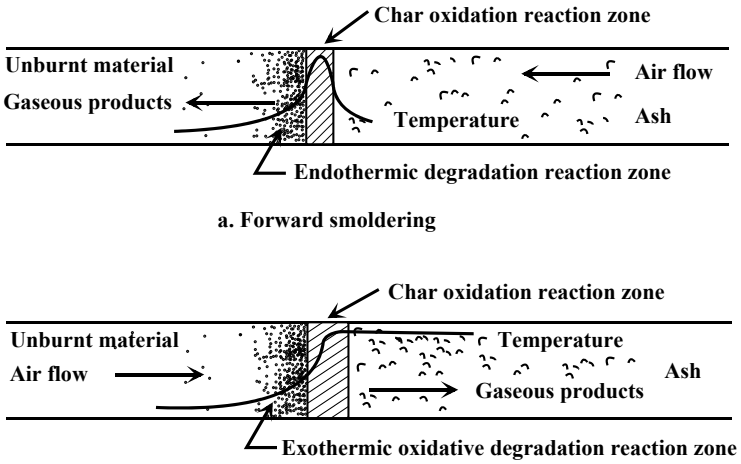

Figure 2.3: Detailed illustration of forward and reverse smoldering. Adopted from Babrauskas [10].

be transported into the degradation zone. The pre-heating of the degradation zone causes the smoldering reaction zone to accelerate [10]. Transition from smoldering to flaming fire has primarily been observed for forward smoldering scenarios [61].

Reverse smoldering

In a reverse smoldering fire, the air moves in the opposite direction of the smoldering reaction zone [57]. The oxygen reaches the reaction zone by moving through the unburnt fuel and the degradation zone. In the smoldering reaction zone, the oxygen reacts with the fuel, producing heat and combustion products. The heat is transported from the reaction zone to the degradation zone, where it pre-heats the fuel. When the fuel reaches the ignition temperature, the reaction zone will move forward [62].

The heat transfer from the smoldering reaction zone to the degradation zone is primarily by conduction and radiation. The air movement from the degradation zone to the reaction zone prevents heat transfer by convection, since it carries heat and combustion products in the opposite direction of the smoldering front [62].

Since the oxygen enters the reaction zone through unaffected fuel, all oxygen will be consumed near the front, leaving unconsumed char in the rear of the reaction zone. The part of the reaction zone where smoldering combustion takes place is narrow compared with the forward smoldering case. Increasing the oxygen supply into the sample reduces the thickness of

the reaction zone and increases the smoldering velocity [14, 62].

Multi-directional smoldering

If smoldering fronts are free to move in several directions, the smoldering reaction zone will be determined by the availability of oxygen [58]. Ohlemiller has reported on 2-dimensional smoldering fronts with strong incline due to spatial variations in the amount of oxygen in a 2D sample of cellulosic insulation [60]. Similar observations were reported by Beever [14].

2.1.3 Smoldering as a surface phenomenon

Smoldering occurs when oxygen reacts with a solid [57]. The reaction occurs at the surface of the material, resulting in gaseous combustion products, char and energy [69]. The char will in some cases undergo a second combustion process often called secondary char oxidation that produces gaseous combustion products, ash and energy [69]. During secondary char oxidation, more energy is produced pr. unit mass than during the primary smoldering combustion [21]. The high energy production combined with a porous char with easy access for oxygen will in some cases result in transition from smoldering to flaming fire. See figure 2.4.

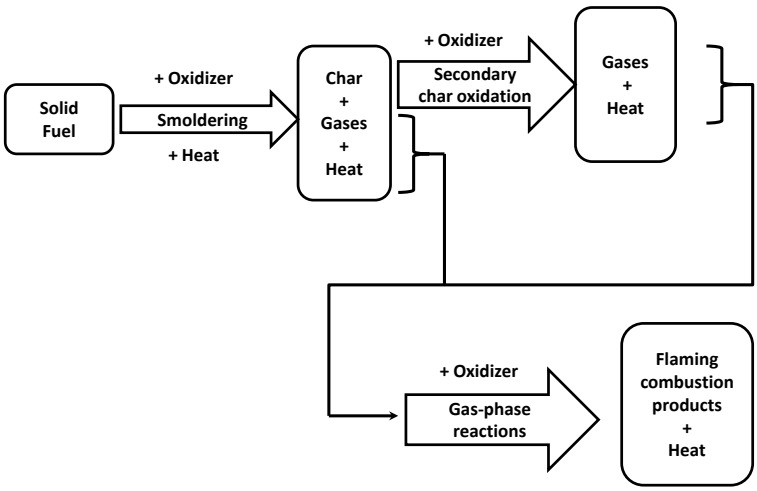

Figure 2.4: Schematic of two typical pathways for a spontaneous transition from smoldering to flaming fire. Adopted from Putzeys [69].

2.2 Factors affecting smoldering

Smoldering is a complex process controlled by the inflow of oxygen and transport of heat away from the smoldering front. Factors like particle size, permeability, density, moisture content and initial temperature will affect both the oxygen transport and heat transfer [24, 62].

2.2.1 Oxygen

In order to maintain smoldering, oxygen must be present in the sample and at the reaction front. Effects of variations in oxygen concentration on the smoldering process have been investigated by Bowes and Thomas [16], Leach et al. [45] and Walter et al. [85]. They show that oxygen both affects the ignition of smoldering and the course of the smoldering reaction. High oxygen concentrations will reduce both time to ignition and the heat flux needed to initiate smoldering, while low concentration of oxygen will increase time to onset of smoldering [85]. When smoldering has been initiated, increased oxygen concentrations beyond standard concentrations (21% O_2) result in higher temperatures in the sample, higher energy production and more complete combustion of the sample material [45].

2.2.2 Density and particle size

Material properties affect the transport of oxygen into the sample. Palmer investigated the effect of particle size of cork dust on smoldering velocity, and found that in still air dust with small particles had a higher smoldering velocity than coarse dust. However, when placed in an air flow, coarse dust had a higher smoldering velocity than finer dust [66].

Given the same density, the oxygen will move more easily into the coarse dust leading to higher smoldering velocity. Investigating the effects of density on smoldering fires in bales of cotton, Wakelyn and Hughs found that at sufficient densities the smoldering fire quenched due to lack of oxygen [84]. Similar results have been reported by Lawson [44].

2.2.3 Layer depth

Layer thickness or depth influences smoldering both during smoldering at the surface of a material or if deep-seated as in a silo [66]. Palmer showed that there is a minimum depth for which smoldering can be sustained [66]. The minimum layer thickness where smoldering can be sustained is dependent on the particle size of the material, the airflow across the sample and properties of the sample. Palmer made the following observations: Smaller particles can sustain smoldering in thinner layers than larger particles. Higher air velocity contributes to sustain smoldering in thinner layers of material. The thinner the material, the higher the relative heat

loss to the substrate, causing a reduction in the smoldering velocity.

The depth of the sample will also affect the smoldering as it propagates through the material. Palmer's experiments show that the time (t) it takes for the smoldering front to move from the bottom of the sample to the top, is proportional to the square of the depth (L) [66].

$$t = \beta \cdot L^2 \tag{2.1}$$

where β is a material-dependent constant, which at the moment can only be determined experimentally [61].

2.2.4 Moisture content

Presence of moisture will affect material properties such as thermal capacity, conductivity and heat of vaporization [10, 24]. Natural occurring materials are often more affected by moisture than man-made materials since these are less hydroscopic [10].

Cellulose materials such as cotton are hydroscopic and will under normal conditions contain 5-10 % condensed moisture [12]. Moisture may occur in porous materials in three forms [40]:

- Free water, which is transported through pores in the material fibers.
- Bound water which is chemically bound to the material fibers.
- Water vapor.

Compared with dry samples, samples containing water will have increased ignition temperature and reduced smoldering velocity [43]. Palmer showed that when the moisture content in sawdust is increased from 0 to 19 %, the smoldering velocity decreased 21 % [66]. Krause and Schmidt reported similar findings for wood dust and dyestuff pigments [43]. Chao and Wang reported that for flexible polyurethane foam the transition from smoldering to flaming fires is impeded by higher moisture contents [21].

The decrease in the smoldering propagation is a result of vaporization of moisture. This process consumes heat which in a dry sample could be used to pre-heat and combust the fuel. Findings by Tran show a decrease in heat release rate as the moisture contents in soft and hard wood increase [80].

The influence of moisture is depended on how fast a material is heated. When a material is rapidly heated by a high heat flux the moisture does not have time to evaporate, resulting in heating both the material and the moisture. The results are increased time to ignition and higher ignition temperature [12]. During slow heating, the moisture will have time to evaporate before

the smoldering front reaches the affected area. Thus, the effects of the moisture are reduced [10, 12].

2.2.5 Initial temperature of material

Results reported by Lupton et al. [49], Rodak et al. [73], Krause and Schmidt [43] indicate that the initial temperature of the sample affects the smoldering velocity and the time to ignition. The smoldering velocity increases as the initial temperature of the material increases [39, 42, 43]. The smoldering velocity may double as the initial temperature increases from 20°C to the self-ignition temperature [43]. Lupton et al. [49] found that the insulation of an electrical wire that did not ignite at ambient conditions, would ignite when exposed to increased temperatures. Rodak et al. [73] found that time to ignition for insulation of an electrical wire would decrease with increasing sample temperature.

2.2.6 Smoldering promoters and inhibitors

Work done on cellulose based materials, shows that there are certain chemical components that will promote or inhibit smoldering. One example is potassium which is a promoter for smoldering in cotton and occurs naturally in cotton [50]. Washing cotton in water will reduce the amount of potassium, reducing or preventing smoldering [38]. The use of sulfur, phosphates and boric acid in cellulose materials, inhibit the smoldering reaction by interfering with free radicals at the smoldering front [10].

2.3 Ignition

Ignition can be described as the transition from a non-reactive decomposition of a material to a self-sustained reactive combustion, The transition is due to an imbalance between the heat production and heat loss in a material [9, 86].

2.3.1 Ignition theory

Ignition models focus on the energy stored in a volume as energy production ($\dot{q}_p$) and energy loss ($\dot{q}_l$) change [37].

$$\text{Change in stored energy} = \text{Energy production} - \text{Energy loss} \tag{2.2}$$

$$\rho C_p V \frac{dT}{dt} = \dot{q}_p - \dot{q}_l \tag{2.3}$$

where: ρ is density, C_p is specific heat, V is volume, T is temperature, t is time, $\dot{q}_p$ is energy production and $\dot{q}_l$ is energy loss.

One of the first ignition models is from Semenov [75]. He considers a volume containing a material that can auto-ignite at certain temperatures. The volumes energy production is based on an Arrhenius approximation [29]:

$$\dot{q}_p = \Delta H_c V C_i A^* e^{-E_a/RT} \tag{2.4}$$

where: ΔH_c is heat of combustion, V is volume, C_i is the concentration of reactants, A^* is pre-exponential factor, E_a is activation energy, R is the universal gas constant and T is temperature. By assuming that none of the material in the volume is consumed prior to ignition, the concentration of reactants in the volume is constant (C_i). Semenov also assumed a uniform temperature in the volume, with the associated heat loss ($\dot{q}_l$) [29].

$$\dot{q}_l = hA(T - T_a) \tag{2.5}$$

where: h is the convection factor, A is the surface area of the volume, T is the temperature and T_a is the ambient temperature. Semenov expanded the plots developed by Taffanel and Le Floch [76], to illustrate the effects of heat production and heat loss as temperature changed in the volume (see figure 2.5).

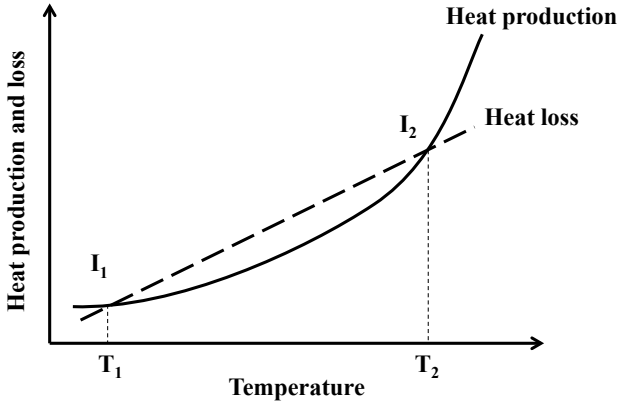

Figure 2.5: Energy production and energy loss as a function of temperature [37].

Two points (I_1 and I_2) on Semenovs plot are of special interest (see figure 2.5). In I_1

the heat production and the heat loss are equal. With temperatures below T_1, the energy production is larger than the heat loss, increasing the temperature in the volume to T_1. With temperature above T_1, but below T_2, the heat loss is larger than the heat production, decreasing the temperature in the volume to T_1. If the temperature in the volume exceeds T_2, the heat production is always larger than the heat loss, resulting in ignition [25].

Semenovs theory is based on a uniform temperature in the volume with a Biot-number (Bi) approaching zero, which indicates a high conduction factor (k) compared with product of the convection factor (h) and the characteristic length of the volume (l) [25]:

$$Bi = \frac{hl}{k} \tag{2.6}$$

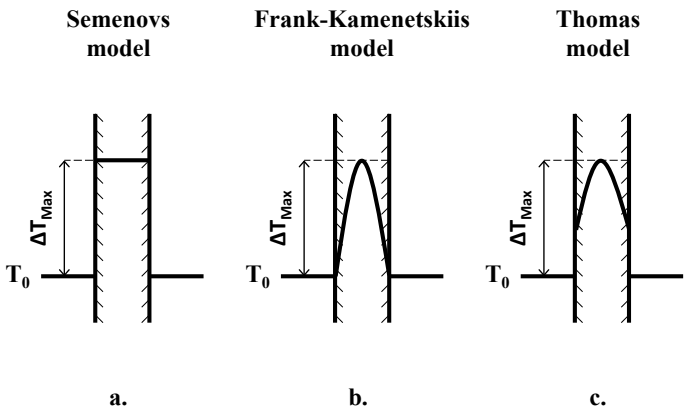

Figure 2.6: Illustration of temperature profiles inside spontaneously-heating volume according to a) Semenov, b) Frank-Kamenetskii and c) Thomas. Adopted from Drysdale [24].

Frank-Kamenetskii evaluated volumes where the convection factor (h) was high compared with the conduction factor (k), and where the Biot-number approaches infinity. With high Biot-number there will be a temperature gradient in the volume [27]. Frank-Kamenetskii introduced a dimensionless heat production factor (δ) which is used in Fourier's heat transfer equation. The heat transfer equation has only solutions when the heating process in the volume is sub-critical, that is no ignition [10]. δ_c indicates a super-critical system where ignition occurs. If $\delta > \delta_c$ then the system is super-critical and ignition occurs [27].

$$\delta = \frac{r_0^2 E_a \Delta H_c A^* C_i^n}{k R T_a^2} e^{(-E_a/RT_a)} \tag{2.7}$$

where r_0 is the characteristic length (see table 2.1), E_a is the activation energy, ΔH_c is the heat of combustion, A^* is the pre-exponential factor, n is the order of the reaction, C is the concentration, k is the conduction factor, R is the universal gas constant, T is temperature in the volume and T_a is the ambient temperature values [25]. δ_c is dependent on the shape of the volume where the heating occurs. In table 2.1 values for different shapes are listed.

Table 2.1: Critical values of Frank-Kamenetskii δ [25].

Shape	δ_c
Slab with thickness $2r_0$	0.88
Sphere with radius r_0	3.32
Cube with side equal to $2r_0$	2.52
Cylinder with radius r_0	2.00

Thomas showed that for small Biot-numbers (0<Bi<10) δ_c is dependent on the Biot-number. This will be the case where both conduction and convection influence the heat transfer in a system [77].

2.3.2 Ignition theory for combustibles on hot surfaces

Semenovs, Frank-Kamenetskiis and Thomas theories are based on uniform heating at all surfaces of a sample. This form of heating is not often encountered in real situations. More common are situations where one side of a sample is heated and others cooled. Examples are dust on hot plates [46, 51], insulation around electrical equipment etc. [55].

Townshend and Bowes developed a solution to the stationary case where one side of a thin layer is kept at a constant high temperature, while the opposite side of the layer is cooled by natural convention [17]. Ohlemiller expanded on Townshend and Bowes theory, developing an ignition model that predicts the ignition temperature for a stationary case [55]. The main assumption of the model is that as long as ignition does not occur, heat from the ignition source and reaction zone is transported to the cooler surroundings. The heat flow balance is given by [55]:

$$\int_{S1} \dot{q}''_{Source} dS_1 + \int_V \dot{q}''' dV = \int_{S2} \dot{q}''_{Loss} dS_2 \tag{2.8}$$

The heat flow balance describes the heat transfer in a control volume limited by the surfaces S1 and S2 (see figure 2.7). In the model developed by Bowes and Townshend [17], S1 is the boundary between the hotplate and the material, while surface S2 is the boundary between the heated material and material at ambient temperature [78]. This is a one-dimensional heat transfer model where heat is only transported up through the material and where heat loss sideways is not accounted for.

The first integral gives the heat flux from the ignition source and into the lower part of the

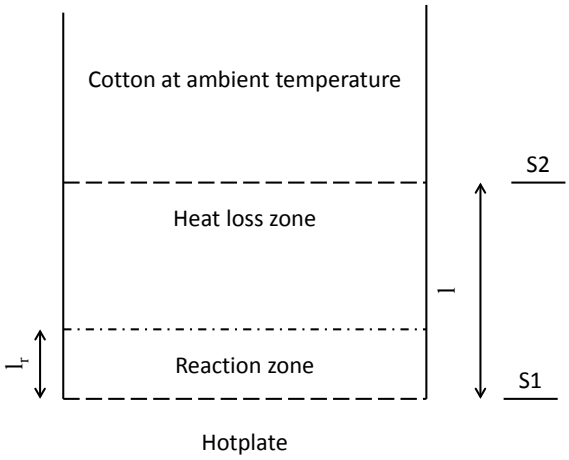

Figure 2.7: Illustration of the one-dimensional heat transfer system.

sample. The second integral gives the heat generated in the material and the third integral gives the heat loss. As the temperature of the ignition source approaches the ignition temperature, the heat production within the material increases. As a result, the temperature in the material will increase and the temperature gradient between the ignition source and material approaches zero [55]. Thus, the first term in eq. 2.8 may be neglected near the ignition temperature, and the equation simplifies to:

$$\int_V \dot{q}'''dV = \int_{S2} \dot{q}''_{Loss}dS_2 \tag{2.9}$$

The heat generation (see eq. 2.10) is assumed to depend on temperature as represented by an Arrhenius function, where the consumption of material is assumed to be zero before ignition [55, 78].

$$\int_V \dot{q}'''dV = \int_0^l \Delta H_c \rho A^* e^{(-E_a/RT(z))}dz \tag{2.10}$$

where ΔH_c is heat of combustion, ρ is density, A^* is a pre-exponential factor, E_a is the activation energy, R is the gas constant, $T(z)$ is the temperature at height z and l is the characteristic length between S1 and S2. Note that the terms in eq. 2.10 give heat flux pr. area, consistent with the 1D-modell. Ohlemiller [55] developed an ignition model based on a constant-temperature reaction zone and a linear temperature gradient in the control volume limited by S1 and S2. The heat generation is dependent on the depth (vertical extension) of the sample reaction zone (l_R) and the constant temperature. It is shown in Appendix A that with a constant temperature in the reaction zone, the right-hand side of eq. 2.10 is approximately given by:

$$\int_0^l \Delta H_c \rho A^* exp^{(-E_a/RT(z))} dz = \Delta H_c \rho A^* l_R exp^{(-E_a/RT_P)} \tag{2.11}$$

where T_P is the hotplate temperature. l_R has the value [55]:

$$l_R = \frac{RT_P^2}{bE_a} \tag{2.12}$$

where b is the temperature gradient in the sample. Ohlemiller's model is based on a stationary situation where the back of the sample is cooled by convection. b is calculated using conduction and convection factors, sample thickness and ambient temperature, assuming a thermally thin material.

$$b = (T_P - T_a)\frac{h}{k}\left(\frac{1}{1+(hl/k)}\right) \tag{2.13}$$

where T_a is the ambient temperature, h is the convection factor, k is the conduction factor and l is the characteristic length.

2.3.3 Onset of smoldering fires

The ignition of a smoldering fire is affected by the same factors as smoldering propagation. In addition characteristics of the ignition source will affect the onset of smoldering.

The shapes and types of ignition sources

Ignition of smoldering fires can be achieved by rising the temperature above a critical level. The temperature rise can be achieved by using hot bodies, thermal radiation or smoldering materials [10].

The geometric shape of the ignition source affects the ignition temperature of the fuel. Ignition sources with different shapes have been tested, and the results show marked differences in the ignition temperature. Ohlemiller studied eight different shaped hotplates as ignition sources when investigating the ignition of cellulose insulation [56]. The results showed a 150 °C difference in ignition temperature as the shape of the ignition source was changed from a corner configuration (lowest) to a wire (highest). Joshi et al. [36] report of similar findings, where a wedge-shape hotplate gives lower ignition temperatures than a flat hotplate. The results of Ohlemiller and Joshi et al. demonstrate that a critical ignition temperature for smoldering is not a unique property of a solid material.

The results of Krause and Schmidt on ignition of cork dust and beech wood dust support the qualitative conclusion from Ohlemiller [41]. In their work Krause and Schmidt used two different ignition sources: heated porcelain spheres and cylindrical wire mesh baskets with dust forming glowing nests. They concluded that the larger the size of the hot body, the lower

the ignition temperature [41].

One of the most commonly used ignition sources in experiments have been cigarettes. The reason is a common fire scenario where cigarettes ignite furniture or bedclothes resulting in fatal fires [30]. Cigarettes are only able to ignite the most reactive gas and liquids. However, cigarettes can initiate smoldering fires and in some cases transition to flaming occur [32].

Smoldering can also be initiated by thermal radiation [15, 28], an additional way for weak ignition sources to cause ignition through smoldering and transition to flaming.

Ignition of smoldering fires does not only depend on temperature, but also on heat flux and exposure time [11].

Oxygen supply and smoldering prohibitors

Different materials have been tested with different concentrations of oxygen [48, 85]. The results show that the oxygen level has little effect on onset of smoldering, but has a strong influence on the smoldering process. Walther et al. [85] showed that oxygen concentration above ambient will decrease ignition temperature and critical heat flux. However, the decrease is not significant. Lohrer et al. [48] found that by lowering the oxygen concentration the self-ignition temperature for coal increases. Oxidation processes in coal were still found at oxygen concentrations as low as 1.3 % [48].

Additives are added to materials to prevent onset of smoldering. Ohlemiller and Rogers [64] found that by adding boric acid to cellulosic insulation, the temperature for onset of smoldering would increase with ca. 20 °C.

Material properties

Variations in material properties are assumed to have little influence on the onset of smoldering. Ohlemiller and Rogers [64] estimated the effect of density, conductivity, convection and ambient temperature on the ignition temperature of cellulosic insulation to be around 10 °C. Badr and Karim show that the ignition of smoldering is delayed as the moisture contains of a material increase [12]. However, more experimental results are needed.

2.4 Transition from smoldering to flaming fire

Transition from smoldering to flaming fire has been found to occur when the smoldering front encounters a different media [6]. Ohlemiller reported that transition to flaming occurred when a smoldering front in cellulose insulation reached the wooden frame of the experiment conducted [59]. Closer investigation of the phenomenon indicates that the cellulose shrinks form-

ing a gap between the cellulous insulation and the wooden frame. An increased flow of air into the reaction zone due to the gap, resulted in an increased heat production. The increased heat production causes glowing and in some cases transition to flaming [10]. The transition from smoldering to flaming is observed to occur in gaps or voids [47, 59].

Glowing or secondary char oxidation has been reported to precede the transition from smoldering to flaming [21, 59, 82]. Tse et al. [82] investigated secondary char oxidation, linking it to the formation of voids in the test sample and increased air supply. The increased air supply results in an increased smoldering rate, but the surplus of oxygen also results in oxidation of char left by the smoldering of the initial material [82].

Putzeys et al. report that the transition to flaming in polyurethane foam occurs in the pores formed by secondary char oxidation in the char region behind the smoldering front [68]. Transition from smoldering to flaming has been observed in samples with large heights. As the smoldering front moves up through the sample, the transition occurs in the char in the lower parts of the sample while the upper part is still smoldering [13, 79].

Experiments on char from polyurethane foam using differential thermal analysis (DTA) showed that heat of combustion for char is 8-10 times higher than for the initial material [21]. The increased heat of combustion is reflected in a higher temperature during secondary char oxidation as compared to the initial smoldering.

Transition from smoldering to flaming has been reported to occur in forward smoldering scenarios, and in reverse smoldering, but only in experimental work [59]. It is not established whether transition to flaming can happen for reverse smoldering in real-life situations [59]. Theoretical work on the transition to flaming has been done by Aldushin et al. [3]. The results show that transition will occur in long samples where the region of char oxidation is heated due to energy transport from lower layers [4]. Aldushin et al. [5] have also looked at models for the transition to flaming for reverse smoldering, and found that for long samples a transition can occur. Computational modeling of transition to flaming has been done by Dodd et al, using Gpyro [23]. The model predicts both time and position of the transition, opening up for the use of modeling in important real-life situations such as domestic fires.

Chapter 3

Experimental set-up

This chapter describes the experimental set-ups used to investigate the onset of smoldering and the transition from smoldering to flaming fire. The material used was cotton.

3.1 Material

The material used in these experiments was cotton batting. Cotton was chosen since it represents a group of cellulose-based materials that are prone to smolder [84]. In addition, cotton is easy to compact to a wanted density. Density was an important parameter in the present study. Commercially available, unbleached cotton batting was used.

During experiments, the ambient temperature was 15-25 °C and the relative humidity 40-50%. Under these conditions cotton has a moisture content of about 5% (by weight). Dry cotton absorbs moisture from the surrounding air as shown in figure 3.1. Since cotton absorbs moisture rapidly and the humidity of the air in the laboratory could not be controlled, it was not feasible to conduct experiments with samples at different moisture contents.

Cotton densities of 5.5, 20, 40, 60, 80 and 100 kg/m^3 were used. Outside this range of densities, the integrity of the experiment could not be upheld: At 5.5 kg/m^3 it was difficult to obtain a homogeneous sample since the cotton became very fluffy. At 100 kg/m^3 it was difficult to compact the cotton without warping the wire mesh container holding the sample.

In table 3.1 porosity and permeability for the different densities are given. The permeability and porosity of cotton were calculated using [54]

$$\kappa = 1.04 \cdot 10^{-11} \frac{\varepsilon^3}{(1-\varepsilon)^{1.22}}, \tag{3.1}$$

$$\varepsilon = \left(1 - \frac{W}{\rho V}\right), \tag{3.2}$$

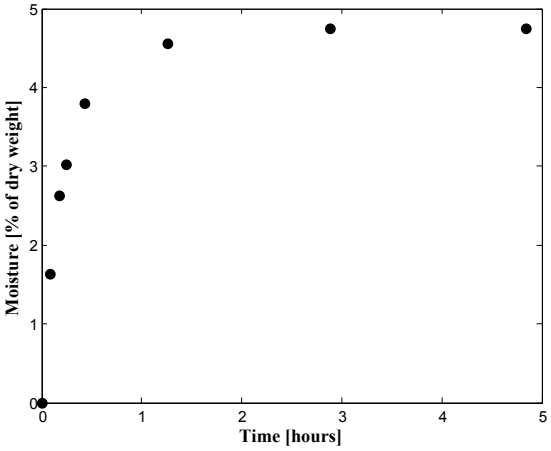

Figure 3.1: Moisture absorption as a function of time for initially dry cotton. Cotton was dried at 100 °C for 12 hours before being exposed to laboratory atmosphere. The dried cotton was placed on a weight, and the mass was recorded.

where κ is permeability, ε is porosity, V is sample volume, W is sample mass and ρ is density.

Since cotton is essentially pure cellulose, the density of cellulose was used for calculating porosity; the density of cellulose is 1440 kg/m^3 [84]. The permeability is reduced by a factor of 40 as the density increases from 5.5 to 100 kg/m^3. In comparison, Putzeys et al. and Torero and Fernandez-Pello used open cell, non-fire retarded polyurethane foam with density 26.5 kg/m^3, porosity 0.975 and permeability $2.76 \cdot 10^{-9}$ m^2 in their experiments on smoldering ignition and propagation [70, 84].

Table 3.1: Calculated values for permeability as a function of sample density, obtained from eq. 3.1 and 3.2.

Density (ρ) (kg/m^3)	Porosity (ε) (-)	Permeability (κ) (m$^2 \cdot 10^{-10}$)
5.5	0.996	91.6
20	0.986	18.4
40	0.972	7.57
60	0.958	4.42
80	0.944	2.98
100	0.931	2.17

Before each experimental run, the cotton was divided into thin layers, packed to a predefined density, and thermocouples placed within the sample (see section. 3.2). If an experiment did not result in smoldering, the cotton was reused. However, the cotton close to the hotplate

was replaced after a non-smoldering experiment since this layer was partly decomposed. The amount of cotton replaced was based on changes in color and texture. In most cases only the lower 2-4 cm of the cotton was replaced.

3.2 Experimental set-up

Two experimental set-ups have been used. The set-ups are closely related.

3.2.1 Set-up for onset of smoldering

This experimental set-up was used to determine the ignition temperature for smoldering in cotton at different densities and heat flux scenarios. The experimental set-up is illustrated in figure 3.2. The test sample was 0.15 m $\times$ 0.15 m $\times$ 0.15 m. The length and width were set by the dimensions of the hotplate plus insulation. The height of the sample was determined from preliminary experiments, where in one case a transition from smoldering to flaming fire was observed when the sample was 0.15 m. Observations by Torero and Fernandez-Pello [79] and Alexopoulos and Drysdale [6] indicate that sample height and gaps in the sample may affect the transition to flaming. In the preliminary test where transition to flaming occurred, the cotton was packed differently from the current samples, with gaps between thick layers of cotton. A main part of the present study focused on the onset of smoldering fires and transition to flaming was therefore undesired. Thus, the height of the test sample was kept at 0.15 m and the cotton was packed without gaps.

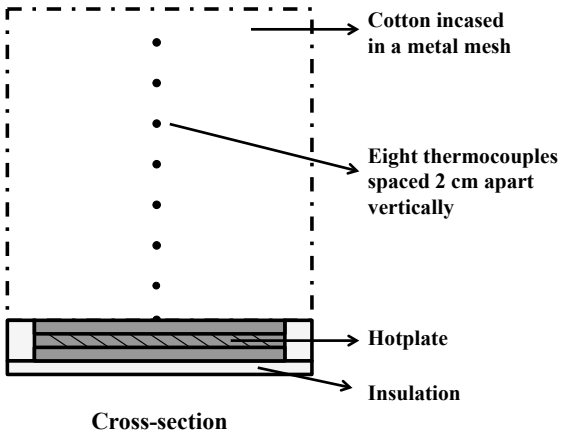

Figure 3.2: First experimental set-up: Test-rig for onset of smoldering fires. The sample consists of cotton packed in a 0.15 m by 0.15 m by 0.15 m metal mesh container. There are eight type-K thermocouples and a hotplate as shown.

Cotton was compacted to a given density, and the sample was held in place using a wire mesh container, as illustrated in figure 3.2. At the top and bottom of the sample, thin metal threads prevented the cotton from expanding. The metal threads and the thermocouples (see below) were used to obtain a homogeneous density throughout the sample. The wire mesh container allowed unrestricted airflow into the cotton. The test-rig was freestanding and air could move unrestrictedly around it. A metal disc formed the bottom side of the container, with good thermal contact between the cotton and the hotplate used as an ignition source.

To monitor the temperature, a type-K thermocouple was placed directly on top of the hotplate. In addition, seven thermocouples were used to measure the temperature within the sample. The thermocouples were spaced 2 cm apart along the vertical centerline of the sample. The thermocouples used had a diameter of 0.5 mm including the outer casing.

A hotplate was chosen as the ignition source, since it allows reproducible heating scenarios. The hotplate consisted of three ceramic tiles, with an electrical hot-wire wound around the middle one, see figure 3.3. The electrical wire yielded 280-285 W, resulting in a temperature rise of 20-30 °C/min at the top of the hotplate.

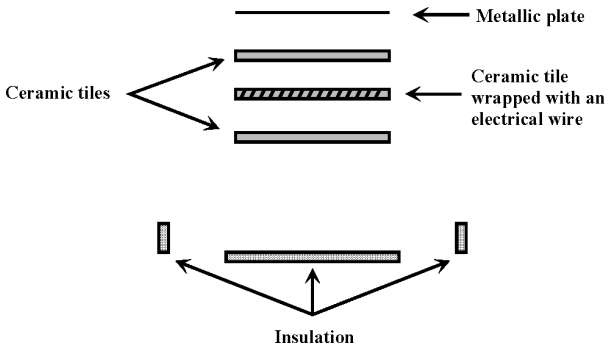

Figure 3.3: Structure of the hotplate (ignition source).

In experiments, the hotplate was heated until the metallic disc reached a pre-determined temperature. Since the center tile was hotter than the top and bottom ones, the measured hotplate temperature increased even after the electrical power was switched off. In figure 3.4a the power was switched off as the hotplate temperature (upper curve) reached 275 °C, while the maximum recorded hotplate temperature was 303 °C. The temperature profile in figure 3.4a is typical for a non-smoldering scenario: the hotplate will cool off after reaching a maximum temperature. Figure 3.4b shows a temperature profile for an experiment where ignition occurred. The hotplate was switched off when the temperature reached 280 °C. Due

to the heat stored in the ceramic tiles, the hotplate temperature continued to increase up to 321 °C, which initiated smoldering. Here the hotplate does not cool off in the same manner, due to the heat production of the smoldering fire, and high temperatures are reached throughout the sample.

In order to reduce effects of air currents, the sample was placed within a container (1.2 m × 0.7 m × 0.6 m) made of light plastic sheets. Before each experimental run cotton was packed to a predefined density and thermocouples placed within the sample. The test-rig was placed on a weight and the mass and the temperature were recorded every 2 seconds during the experiments.

3.2.2 Set-up for transition from smoldering to flaming fire

This second experimental set-up was used to investigate how boundary conditions affect the transition from smoldering to flaming fire. Two different boundary conditions were tested: open boundaries (as described in section 3.2.1) and an additional wall made of a lightweight concrete block. Transition from smoldering to flaming fire was not observed in the experiments for onset of smoldering, described in section 3.2.1. To avoid effects of sample height, the same height as in section 3.2.1 was chosen for the experiments described below.

To monitor the temperature, a type-K thermocouple was placed directly on top of the hotplate. In addition, 35 thermocouples were used to measure the temperature within the sample. At every 2 cm vertically, 5 thermocouples were placed, forming a cross (see figure 3.5b); 4 thermocouples were placed 3.75 cm from the thermocouple at the vertical centerline of the sample. At heights 6, 8, 10 and 12 cm from the hotplate, an additional thermocouple was placed between the cotton and the boundary. In the cases with no boundary material (open boundary) the thermocouples were placed at the surface of the cotton. The thermocouples used had a diameter of 0.5 mm including the outer casing. The number of thermocouples was increased from 8 to 40 to get a better understanding of how the smoldering front moved when affected by the boundary.

In order to reduce effects of air currents, the sample was placed within a container (1.2 m × 0.7 m × 0.6 m) made of light plastic sheets. Before each experimental run cotton was packed to a predefined density and thermocouples placed within the sample.

The test-rig was placed on a balance and the mass and the temperatures were recorded every 3 seconds during the experiments. The time interval was increased from 2 seconds (for the experiments described in section 3.2.1) to 3 seconds to have time to read the increased number of thermocouples. The same hotplate as described in section 3.2.1 was used in these experiments.

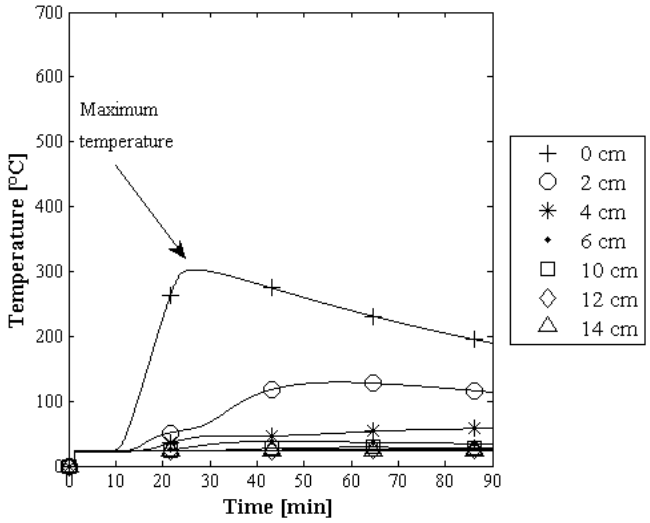

a. Non-smoldering scenario

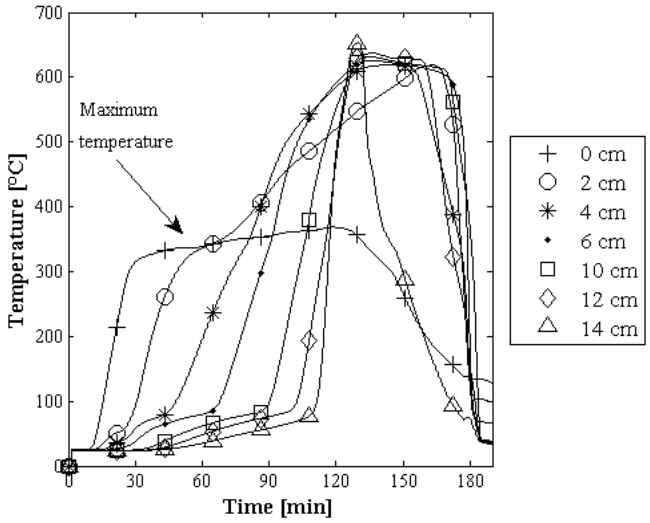

b. Smoldering scenario

Figure 3.4: Temperatures as function of time for a non-smoldering (upper plot) and a smoldering scenario (lower plot) with cotton density 100 kg/m^3. Each curve shows temperatures measured at a given vertical distance above the hotplate, see figure 3.2. Distance 0 cm is the hotplate temperature.

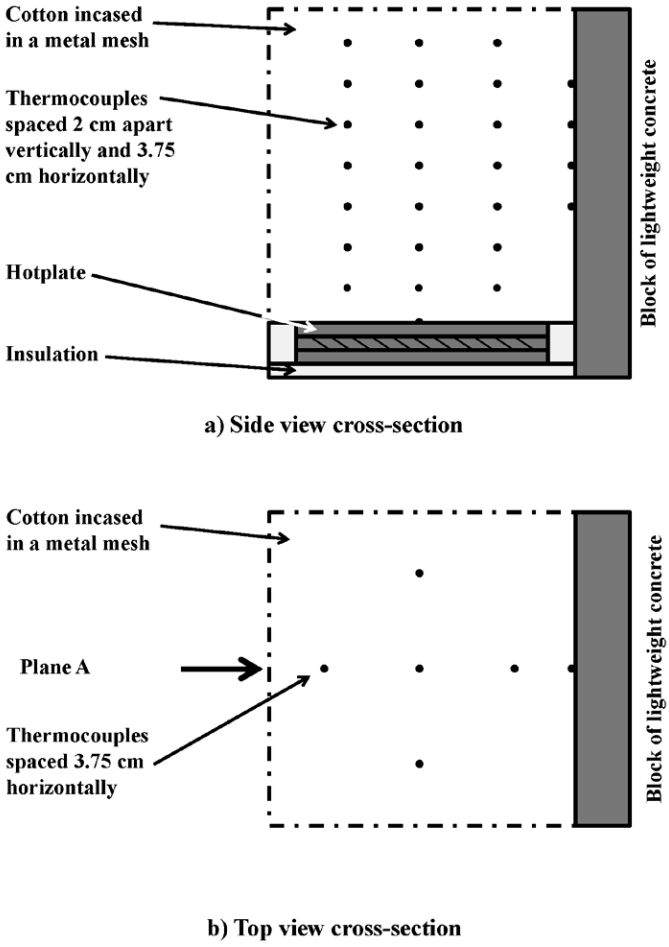

Figure 3.5: Second experimental set-up: The cotton sample was incased in a metal mesh container with a lightweight concrete block at one of the boundaries. At every 2 cm vertically in the sample there were placed five type-K thermocouples forming a cross. The thermocouples in each layer were placed 3.75 cm from each other horizontally. The hotplate consisted of three ceramic tiles, with an electrical hot-wire wound around the middle one.

3.3 Experimental procedures

The experimental procedures for studying the onset of smoldering and the transition from smoldering to flaming are described below.

3.3.1 Onset of smoldering

Six different heat flux scenarios have been investigated to get a better understanding of how the heating mode and density affect the onset of smoldering (see figure 3.6). Scenario A represents fast heating of a sample with subsequent cooling of the hotplate. This type of heating happens when an ignition source is in contact with a material and then removed. Scenario D represents a slow heating of a sample over a long period of time. This is representative where a material is placed on a heated surface for a prolonged period of time. Scenarios B and C are heating scenarios between A and D, with lower heat flux than in scenario A but for extended and finite time periods. Scenario E combines scenarios A and D. Scenario F represents situations with materials that are repeatedly heated and cooled, which may occur if a material is left for example on an engine. The six heating scenarios are described in more detail below.

Scenario A. High heat flux followed by cooling: The hotplate was heated to a pre-determined temperature (called the cut-off temperature), and then switched off. A heat flux of 12.8 kW/m^2 (the maximum allowed by the current set-up) was used, resulting in a temperature rise of 20-30 °C pr. minute at the top of the hotplate (see figure 3.6). In figure 3.7a the power was switched off as the hotplate temperature (upper curve) reached 275 °C, while the maximum recorded hotplate temperature was 303 °C.

The temperature profile in figure 3.7a is typical for a non-smoldering experiment: here the hotplate will cool after reaching a maximum temperature. In figure 3.7b the power was switched off as the hotplate temperature (upper curve) reached 280 °C, and the increased hotplate temperature (as compared with the case in figure 3.7a) resulted in ignition. Here the hotplate does not cool, due to the heat production of the smoldering fire, and high temperatures are reached throughout the sample.

Scenario B. Medium high heat flux followed by cooling: The hotplate was heated to a pre-determined temperature, and then switched off. A heat flux of 4.5 kW/m^2 (35% of the flux for scenario A) was used, resulting in a temperature rise of 7 °C pr. minute at the top of the hotplate. In figure 3.7c the hotplate was switched off when the temperature reached 305 °C, giving a maximum temperature of 311 °C which did not cause ignition. In figure 3.7d the hotplate reached a maximum temperature of 316 °C, initiating smoldering.

Scenario C. Medium low heat flux followed by cooling: The hotplate was heated to a pre-determined temperature, and then switched off. A heat flux of 2.22 kW/m^2 (18% of the flux for scenario A) was used, resulting in a temperature rise of 3 °C pr. minute at the top

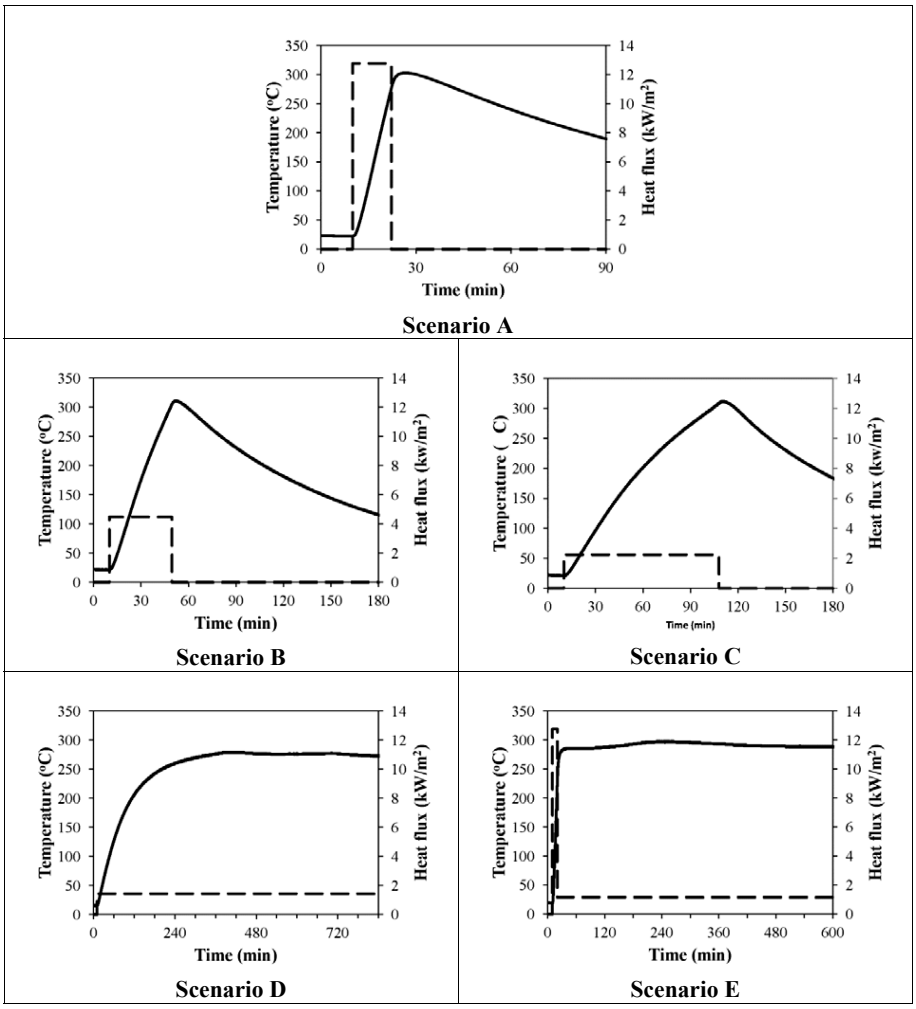

Figure 3.6: Heat flux and hotplate temperature as a function of time for the scenarios used in the experiments. Scenario F is not shown since it is a series of scenario A experiments. The hotplate was heated as indicated by the dotted line, resulting in a hotplate temperature as indicated by the solid line. Density was 100 kg/m^3.

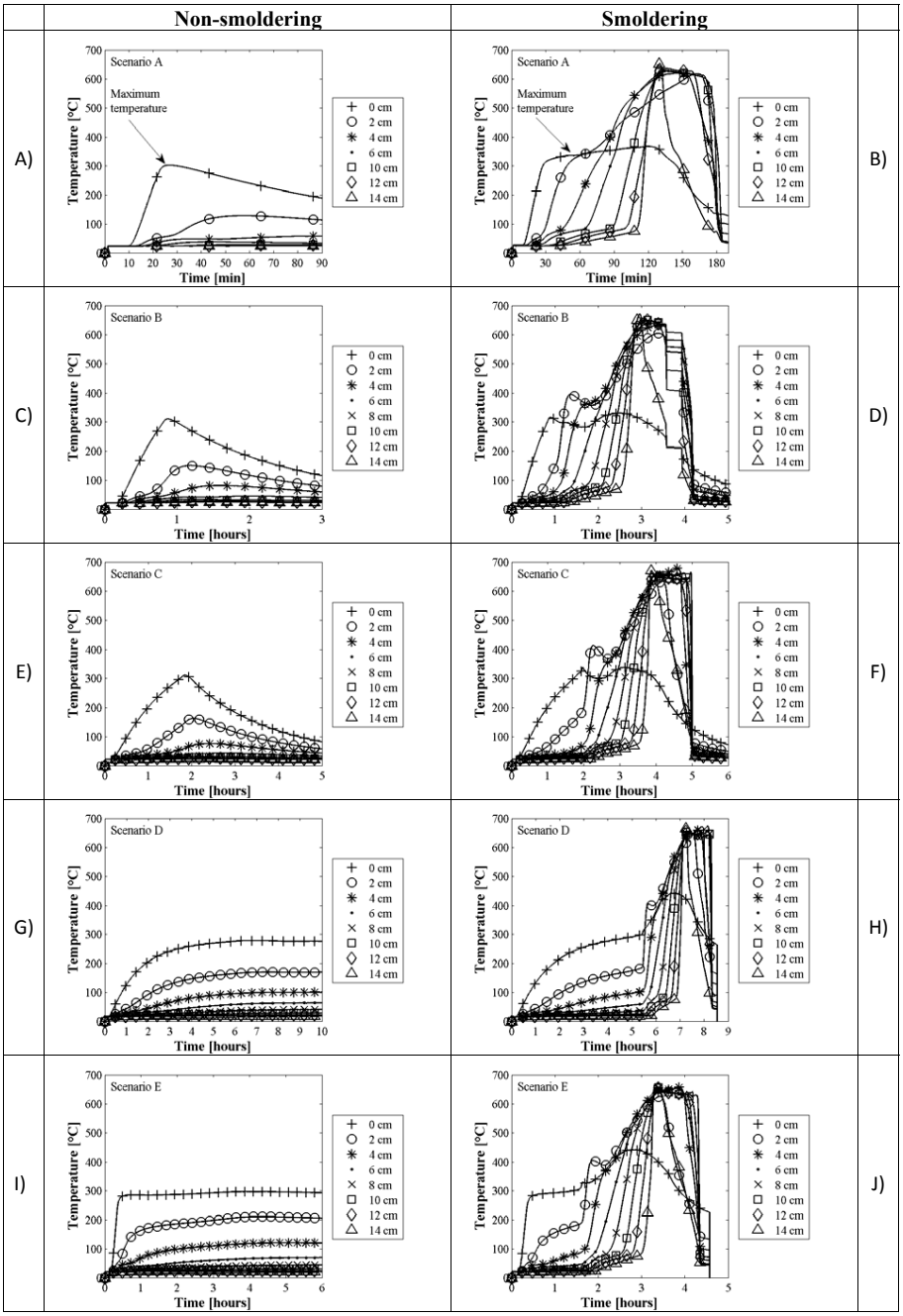

Figure 3.7: Temperatures as a function of time and position for scenarios A-E for both non-smoldering (left column) and smoldering cases (right column). The temperature was measured at the hotplate (0 cm) as well as at a series of different heights above it, as indicated. The density was 100 kg/m^3. In scenario B, part (D), some data are missing after the maximum is reached.

of the hotplate. The temperature curves for a non-smoldering case are shown in figure 3.7e. The hotplate reached a maximum temperature of 312 °C, with no smoldering. In figure 3.7f the hotplate was switched off at 315 °C. In this case the temperature did not stabilize and smoldering occurred.

Scenario D. Low constant heat flux: The sample was heated using a low constant heat flux. Figure 3.7g shows the temperature development for an experiment where the power was held constant at 1.43 kW/m^2, resulting in a maximum hotplate temperature of 279 °C with no onset of smoldering. Due to the constant heat flux, the temperature stays constant when the maximum temperature has been reached, in contrast to the non-smoldering cases in scenarios A-C, where the temperature is reduced when the hotplate is switched off. An increase in the power input to 1.52 kW/m^2 resulted in ignition, as shown in figure 3.7h.

Scenario E. High heat flux followed by low constant heat flux: The hotplate was heated rapidly using a heat flux of 12.8 kW/m^2, as for scenario A. As the hotplate reached a pre-determined temperature of 230 °C the power input was reduced to a low constant heat flux. In figure 3.7i the heat flux was reduced from 12.8 to 1.16 kW/m^2 as the hotplate temperature (upper curve) reached 230 °C, while the maximum recorded hotplate temperature was 297 °C. The temperature profile in figure 3.7i is typical for a non-smoldering experiment. In figure 3.7j the heat flux was reduced from 12.8 to 1.25 kW/m^2 as the hotplate temperature reached 230 °C; the temperature did not stabilize resulting in ignition. 230 °C was chosen as the temperature at which the heat flux was reduced since cotton at this temperature will discolor but not decompose.

Scenario F. Multiple heating and cooling: In this scenario a sample was heated and cooled multiple times. No cotton was replaced between experiments. The hotplate was heated until it reached a pre-determined temperature, and then power was switched off as described for scenario A. If no ignition occurred the sample was allowed to cool down to ambient temperature and then re-heated to a new, pre-determined and higher cut-off temperature. The increase in hotplate temperature between runs was 5 °C, and the re-heating continued until ignition occurred.

Before the data acquisition began, the power supply for the hotplate was turned on and the sample placed on the hotplate. When the systems had stabilized, ten minutes of background data was collected (see figures 3.6 and 3.7). After ten minutes, the hotplate power was increased from zero to a pre-determined value. In scenarios A, B, C and F the power was switched off when the hotplate reached a pre-determined temperature called the cut-off temperature. Due to the high core temperature of the hotplate, the temperature at the top of the hotplate increases beyond the cut-off temperature in all these cases. The maximum hotplate temperature was recorded. In scenarios D and E the power to the hotplate was not switched off, and temperatures tend to stabilize for non-smoldering cases.

If smoldering was observed the test was terminated when the char and ash of the cotton had cooled down to less than 100 °C. If smoldering was not observed, the test was terminated when both the thermocouple on top of the hotplate and the one 2 cm above the hotplate showed decreasing temperatures. In the present work, the cut-off and the maximum temperatures (both referring to the hotplate) were used to determine the ignition temperature for scenarios A, B, C and F (see section 4.2). For scenarios D and E the heat flux and the maximum temperature of the hotplate were used to estimate the ignition temperature.

When a test did not result in smoldering the cut-off temperature was increased with 5 °C in the subsequent experiments for scenarios A, B, C and F. For scenarios D and E the heat flux was increased with 0.09 kW/m^2, which was the lowest increment possible for this experimental set-up.

3.3.2 Transition from smoldering to flaming fire

Two different boundary conditions have been investigated, representing cases where it is expected that both heat transfer and transport of oxygen into the cotton differ.

Open boundary: In this case all sides and top of the sample were open to the ambient air. The air could move freely into the cotton, and the heat transfer from the cotton to the surroundings was unrestricted (see figure 3.2).

Lightweight concrete block: In this case one side of the cube was covered by a lightweight concrete block (see figure 3.5). The block prevented air from entering the sample through the covered side and also acted as a heat sink. The lightweight concrete block had a density of 500 kg/m^3, specific heat of 1.1 kJ/kgK and conductivity of 0.144 W/mK.

Before data acquisition began, the power supply for the hotplate was turned on at negligible power (0 W/m^2) and the compacted cotton placed on the hotplate. When the system had stabilized, ten minutes of background data was collected. After ten minutes, the hotplate power was increased to 12.8 kW/m^2 (similar too scenario A). The power was switched off when the hotplate-temperature reached a pre-determined temperature of 330 °C, called the cut-off temperature. For this experimental set-up, onset of smoldering occurs between 280 and 340 °C (see table 4.1). The cut-off temperature of 330 °C was chosen since the high core temperature of the hotplate would assure temperatures above the temperatures for onset of smoldering. Data acquisition was stopped when the char and ash of the cotton had cooled down to less than 100 °C.

Chapter 4

Experimental results

4.1 Recorded data

The temperatures at the hotplate and along the centerline of the cotton were measured to determine onset of smoldering (see figure 3.4). Figure 3.4a shows temperature as a function of time for a non-smoldering scenario, while figure 3.4b shows a smoldering scenario. The temperatures for the non-smoldering case increase and decrease systematically, and the temperature decreases with distance from the hotplate. The temperatures for the smoldering case are more erratic since the smoldering process dominates as heat source. Smoldering also results in higher temperatures. As the cotton was consumed, the thermocouples were exposed to cold air, resulting in rapidly decreasing temperatures. In cases with smoldering, the temperatures in figure 3.4b evolve in a way that is independent of the heat scenario. On the other hand, the time to onset of smoldering depended on scenario.

The temperatures for a case with transition to flaming initially behaves as a pure smoldering case (see figure 4.1a): a systematic increase in temperatures followed by a more erratic behavior as smoldering occurs. At the transition from smoldering to flaming even more erratic temperature changes can be observed due to the presence of flames, as shown in figure 4.1b. For the investigation of transition to flaming, the temperature in the cotton was measured at several positions, as described in section 3.2.2.

At temperatures between 40 and 80 °C, a lower temperature gradient is observed (see figure 4.1a). This is probably due to evaporation of moisture in the cotton. A lower temperature gradient is consistent with observations on heated sawdust [17] and polyurethane foam [8]. The presence of moisture should be included when modeling onset of smoldering, as described in chapter 5.

The sample mass as a function of time was recorded, as shown in figure 4.2. The sample mass decreases systematically with time. A constant mass loss rate can be extracted as a first

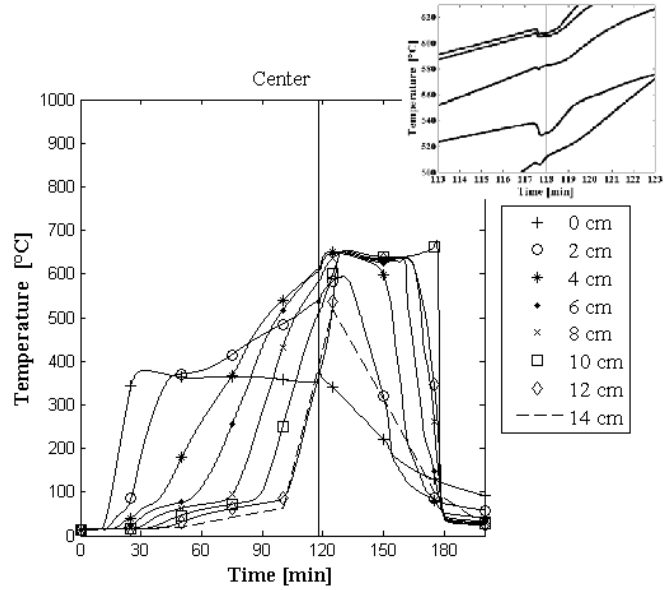

a) Centerline temperature

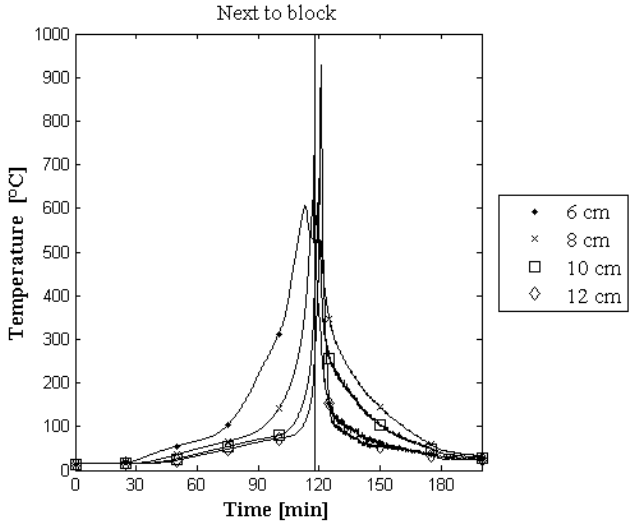

b) Temperature at boundary of lightweight concrete

Figure 4.1: Temperature as a function of time for a smoldering scenario where transition to flaming occurs. Sample density was 80 kg/m^3. Part (a) shows the temperatures along the vertical centerline, while part b) shows the temperatures at the boundary between the cotton and the lightweight concrete block. The insert in part (a) shows the erratic temperature when glowing and flaming occur at 118 minutes (indicated by the vertical line in the plot). Each curve shows temperatures measured at a given vertical distance above the hotplate.

approximation. The mass loss rate due to smoldering increases with increasing sample density (see table 4.4).

The movement of the smoldering front along the outside of the sample was recorded by a photo every minute, see figure 4.3. In figure 4.3a a case leading to flaming is shown, while figure 4.3b shows a pure smoldering case not leading to flaming. The effects of the differences in the smoldering fronts are discussed in chapter 6. Glowing, transition to flaming and extinguishment were short-lived processes during the current experiments and video filming was used to document them.

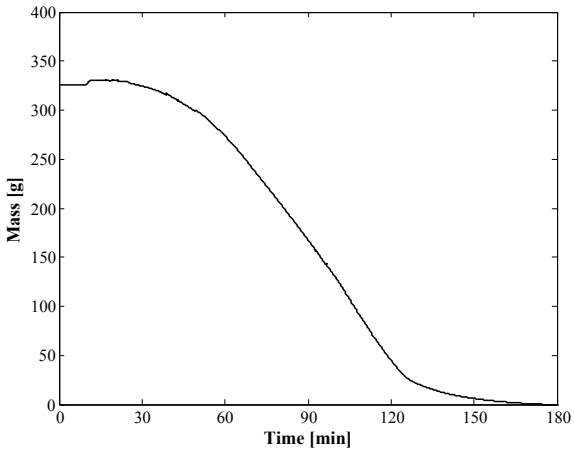

Figure 4.2: Sample mass as a function of time for density 100 kg/m^3. Measured temperatures for this experiments are shown in figure 3.4b (Scenario A: high heat flux followed by cooling).

4.2 Onset of smoldering

From temperature plots like those shown in figure 3.4, the maximum temperature of the hotplate is found. For the non-smoldering cases, the maximum hotplate temperature is determined as the point where the hotplate temperature first levels out and starts to decrease (see scenario A in figure 3.7a). For the smoldering cases the maximum hotplate temperature is taken as the point where the hotplate temperature levels off (see scenario A in figure 3.7a) or where the hotplate temperature has a significant increase, as shown for scenario D in figure 3.7h. The maximum hotplate temperature as a function of cut-off temperature for different scenarios is plotted in figure 4.4. Each plot represents a series of experiments with the same density and heat flux scenario.

There is a linear relationship between the cut-off temperature and the maximum hotplate

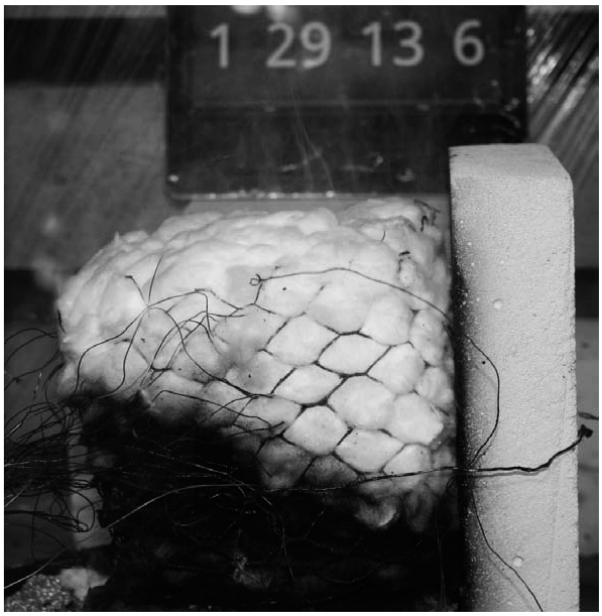

a) Smoldering case with tilted front leading to transition to flaming

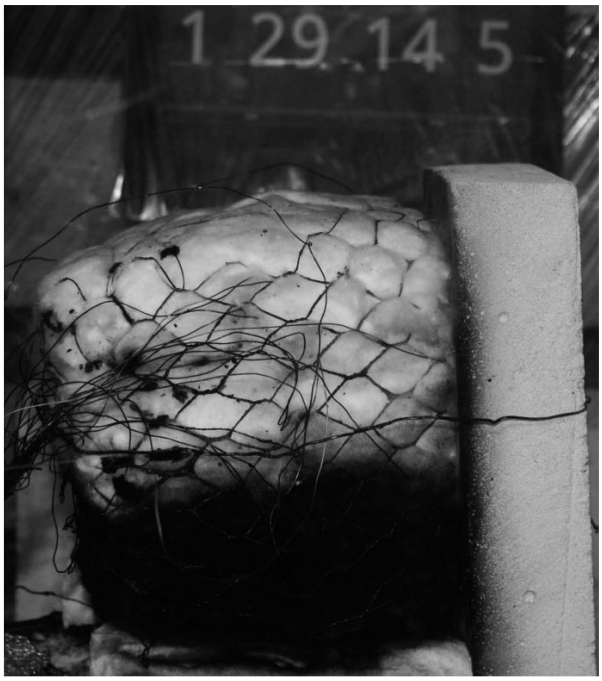

b) Pure smoldering case with horizontal front

Figure 4.3: The smoldering fronts for a case leading to flaming and a case with pure smoldering differ. The sample density was 100 kg/m^3 in both cases. The boundary condition was defined by a block of lightweight concrete at the right side of the sample.

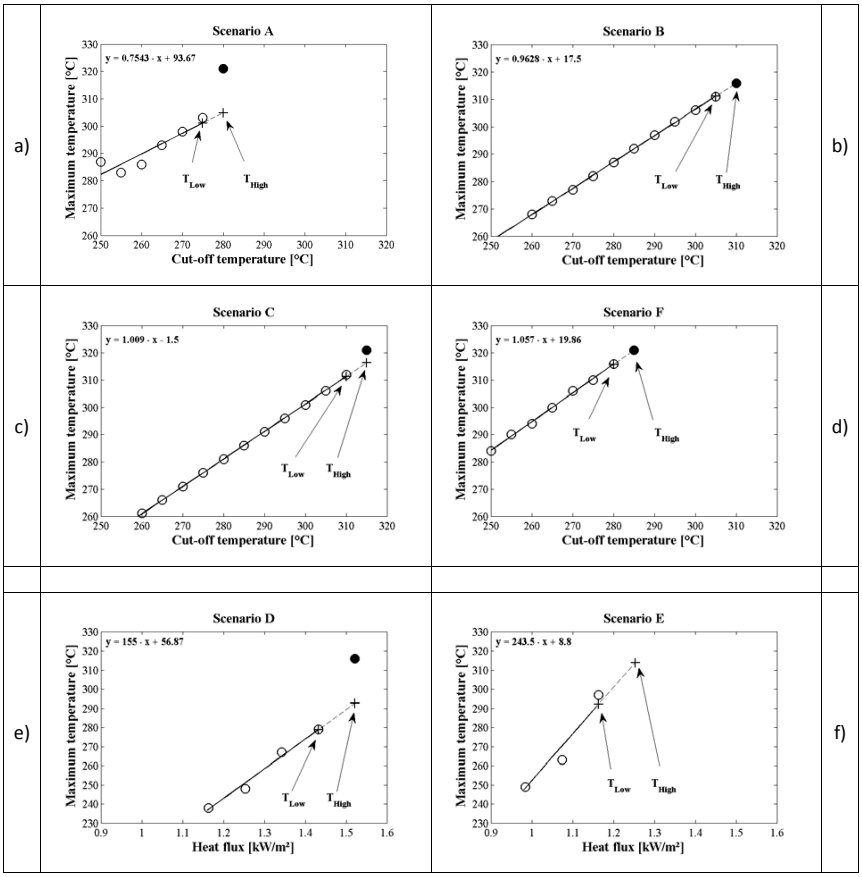

Figure 4.4: Maximum hotplate temperature as a function of cut-off temperature or heat flux for a series of experiments at density 100 kg/m^3. In each part, the line is a linear fit to all points corresponding to non-smoldering cases. The smoldering case is indicated by a solid circle (•) while the non-smoldering cases are indicated by circles (○). T_{High} and T_{Low} are indicated by a crosses (+). These quantities extracted from the data are discussed in the main text.

temperature for the non-smoldering cases, while the case where smoldering occurs deviates significantly (see figure 4.4a-d). Using the linear fit for the non-smoldering cases an upper bound, T_{high}, and a lower bound, T_{low}, for the temperature-interval where ignition occurs, can be determined from plots like those in figure 4.4. Using the linear fit and the cut-off temperature for the last non-smoldering case, T_{low} is estimated as a lower temperature limit for the ignition interval (301 °C for scenario A in figure 4.4a). Similarly, using the linear fit and the cut-off temperature for the cases causing smoldering, T_{high} is estimated as an upper temperature limit for ignition interval (305 °C for scenario A in figure 4.4a). It is reasonable to assume that ignition occurred between T_{high} and T_{low}. The values for T_{high} and T_{low} for different scenarios are shown in figure 4.4a - 4.4d. The temperature for onset of smoldering is estimated as the average of T_{high} and T_{low} and listed in table 4.1.

There is also a linear relationship between the heat flux and the maximum hotplate temperature (see figure 4.4e-f). For the heat flux scenarios with constant low heat flux (scenarios D and E) the maximum hotplate temperature is the approximately constant value reached after a sufficient time (see figure 3.7). In figure 4.4e and f the maximum hotplate temperature is plotted against the power output from the hotplate to estimate the ignition temperature for scenarios D and E. A similar procedure as described for maximum hotplate versus cut-off temperature was used to determine T_{low}, a lower bound for the ignition temperature (279 °C for scenario D in figure 4.4e) and T_{high}, an upper bound for the ignition temperature (289 °C for scenario D in figure 4.4e). The temperature for onset of smoldering is given in table 4.1.

Six different heating scenarios have been studied, using densities from 20 - 100 kg/m^3. Table 4.1 shows that both density and heating scenarios affect the onset of smoldering. The higher the density, the lower the temperature for onset of smoldering. The scenarios with slow heating of the sample (scenarios D and E) have lower temperature for onset of smoldering than for scenarios where the sample is heated more quickly. Scenario F with multiple heating of the same sample has a significant higher temperature for onset of smoldering than the samples that were only heated once. Table 4.2 shows that a heat flux as low as 1.21 kW/m^2 can induce smoldering in cotton. A general trend is that higher density samples need less heat flux to smolder.

4.3 Transition from smoldering to flaming

In the current experiments, a transition from smoldering to flaming fire only occurred for cases where a lightweight concrete block covered one side of the cotton sample (see table 4.3). Prior to the transition, the smoldering front had consumed the outer parts of the sample (see figure 4.5), leaving a region of warm un-combusted cotton next to the concrete block (see figure 4.6a). Thereafter high-temperatures reaction fronts formed as small glowing embers could be observed in the char behind the smoldering front. The embers moved erratically along

Table 4.1: Ignition time and temperature as a function of density and scenario.

	Scenario					
	A High heat flux followed by cooling	B Medium high heat flux followed by cooling	C Medium low heat flux followed by cooling	D Low constant heat flux	E High heat flux followed by low constant heat flux	F Multiple heating and cooling of the same sample
Density (kg/m^3)	(°C) (min)	(°C) (min)	(°C) (min)	(°C) (min)	(°C) (min)	(°C) (min)
5.5	*	-	-	-	-	-
20	307 ±2 (16)	- -	- -	306±4 (151)	336± 4 (60)	- -
40	318 ±3 (17)	- -	- -	320 ±6 (192)	302 ±7 (52)	338 ±2 (16)
60	315 ±2 (17)	- -	- -	319 ±7 (259)	305 ±10 (98)	- -
80	309 ±2 (17)	- -	- -	305 ±5 (328)	300 ±10 (96)	- -
100	303±2 (18)	313 ±2 (41)	314 ±2 (99)	284 ±5 (256)	303 ±11 (79)	319 ±2 (16)

* No ignition
- Not investigated
() Time to onset of smoldering

Table 4.2: Minimum heat flux to initiate ignition of cotton.

	Scenario	
	D Low constant heat flux	E High heat flux followed by low constant heat flux
Density (kg/m^3)	(kW/m^2)	(kW/m^2)
5.5	-	-
20	1.83 ± 0.04	2.10 ± 0.04
40	1.66 ± 0.04	1.30 ± 0.04
60	1.57 ± 0.04	1.21 ± 0.04
80	1.66 ± 0.04	1.21 ± 0.04
100	1.48 ± 0.04	1.21 ± 0.04

- Not investigated

treads of charred cotton. At this point, in some but not all experimental runs, a transition from smoldering to flaming was observed. The flames lasted for 0.5 - 2 minutes. After flaming had ended, the sample continued to smolder, consuming the remaining fuel in the sample.

Table 4.3: Observed transition from smoldering to flaming as a function of density and boundary. The results for the open boundary are from one experiment, while the total numbers of experiments with a lightweight concrete block are given in parentheses.

	Boundaries	
Density (kg/m^3)	Open	Light weight concrete block
20	No	No (5 tests)
60	No	Yes (2 tests) (117 min)
80	No	Yes (3 tests) (118 min)
100	No	Yes (4 tests) (133 min)
( ) Time to transition from smoldering to flaming fire		

When comparing temperature contour plot for a case with transition to flaming (see figure 4.6a) with a pure smoldering case (see figure 4.6b), subtle differences in the temperature distribution can be observed as shown in figure 4.7: the temperature close to the lightweight concrete is higher for the pure smoldering case than for the case with transition to flaming. In figure 4.8 temperature contour plots for a case with open boundaries are shown at 90 and 100 minutes. Figure 4.8a shows a more homogeneous temperature evolution spatially in the cotton sample compared with figure 4.6a, and that the whole sample was smoldering at 100 minutes (see figure 4.8b). The effect of the lightweight concrete block is apparent, with tilted smoldering fronts in figures 4.6a, while in figures 4.6b and 4.8 the smoldering front moves more evenly up through the sample.

The intense, high-temperatures reaction fronts were observed in all cases where the transition from smoldering to flaming fire occurred, but also in cases where flaming did not occur. These reaction fronts, often referred to as secondary char oxidation, have previously been associated with the transition from smoldering to flaming fire [61, 67, 68]. The time at which the secondary char oxidation occurs is important. In the flaming cases, the secondary char oxidation occurred before all the warm cotton in the region 8-12 cm above the hotplate and towards the block (see figure 4.7) was consumed, while for the non-flaming cases the char oxidation occurred after the cotton was consumed. For the case in figure 4.6a the secondary char oxidation occurred at 116 min and flaming occurred at 117 min. For the non-flaming case in figure 4.6b the char oxidation occurred at 144 min, at which all the cotton was consumed by the smoldering front.

Figure 4.5: Photo of the cotton cube with density 60 kg/m^3 at 100 minutes, 17 minutes before transition to flaming occurred. The smoldering front has consumed the outer part of the cotton sample. The temperature profile in the cotton is shown in figure 4.6a.

The transition from smoldering to flaming fire in the current experiments has been observed for densities 60, 80 and 100 kg/m^3, but only when one of the boundaries of the sample was covered by a lightweight concrete block (see table 4.3). For density 20 kg/m^3 and for open boundaries, flaming combustion has not been observed. Thus, both the boundary conditions (all sides of the sample open versus block at one side) and density influence the transition from smoldering to flaming.

4.4 Mass loss rate

4.4.1 Mass loss rate as a function of density and scenario

Sample mass as a function of time is shown for scenario A and several densities in figure 4.9, and in figure 4.10 for several scenarios and density 100 kg/m^3. The mass loss rates with density 100 kg/m^3 are shown in figure 4.11. The mass loss rates are changing during the entire smoldering process. The heat flux scenario affects the time to onset of smoldering, but subsequently the mass loss rate is independent of the scenario. The maximum mass loss rate is approximately the same for the six cases and occurs when the smoldering front has moved up 10 cm through the cotton cube (see table 4.4).

An average mass loss rate for the different scenarios and densities can be found from the time it takes to reduce the mass from 90 to 10 % of the initial values. The average mass

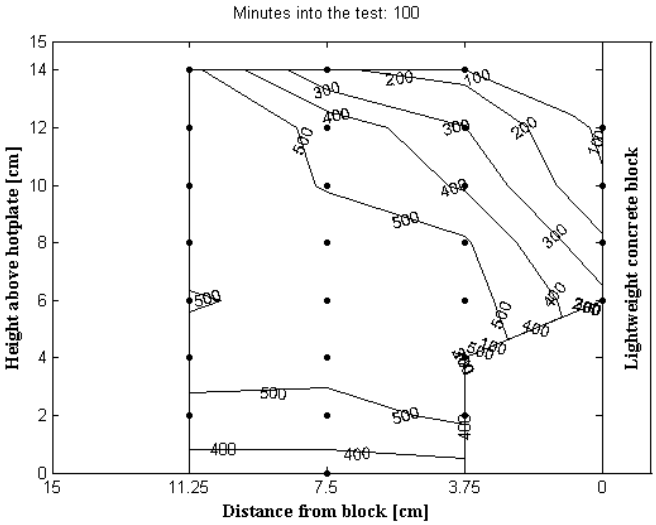

a. Smoldering case with transition to flaming

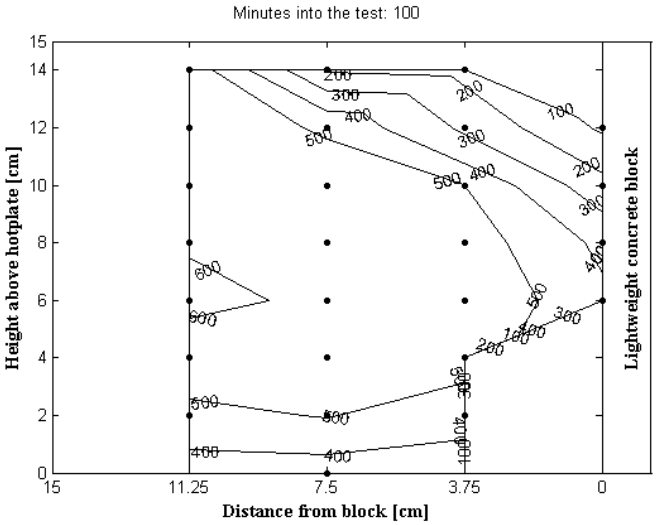

b. Pure smoldering case with no transition to flaming

Figure 4.6: Temperature contour plots of a smoldering case with transition to flaming (part(a)) and a pure smoldering case (part (b)). Sample density was 60 kg/m^3. Part (a) shows the temperature in plane A (see figure 3.5) in the cotton 17 minutes before secondary char oxidation and flaming occur. The outer layers of the cotton have been consumed by the smoldering front (see figure 4.5), while the region next to the concrete block is warm but not consumed. The estimated temperature for onset of smoldering is 315 °C for cotton with density 60 kg/m^3 (see table 4.1). The plots show isolines for temperatures at every 100 degrees between 20 and 600 °C. Part (b) shows the temperature in plane A at 100 minutes, similar to figure part (a). This case will only smolder, and the smoldering front has reached higher into the region next to the concrete block. The lightweight concrete block is at the right of the plot and the positions of the thermocouples are indicated by dots.

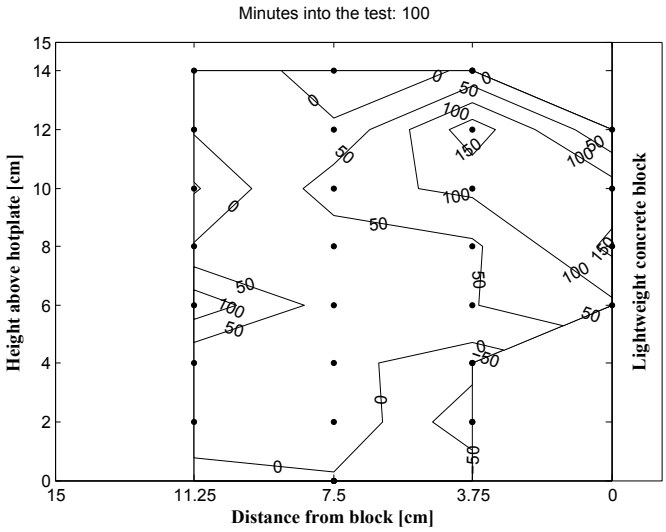

Figure 4.7: Temperature-difference contour plot of cases with density 60 kg/m^3. The plot shows the temperature difference between figure 4.6a and 4.6b in plane A (see figure 3.5) at 100 minutes (temperatures in figure 4.6b minus temperatures in figure 4.6a). Positive values indicate that the pure smoldering case has higher temperature than the smoldering case leading to flaming. The plot shows that 8 to 12 cm above the hotplate and towards the concrete block, the temperature for the smoldering case leading to flaming is 100 - 150 °C lower than the pure smoldering case. The lightweight concrete block is at the right of the plot and the positions of the thermocouples are indicated by dots.

Table 4.4: Maximum mass loss rate for the cases shown in figure 4.11.

Scenario	Maximum mass loss rate	Time for occurrence of maximum mass loss rate	Time for smoldering front to move up 10 cm in the cotton cube
	(g/min)	(min)	(min)
A	3.98	93	103
B	4.32	145	145
C	4.18	205	201
D	4.18	403	401
E	4.62	173	170

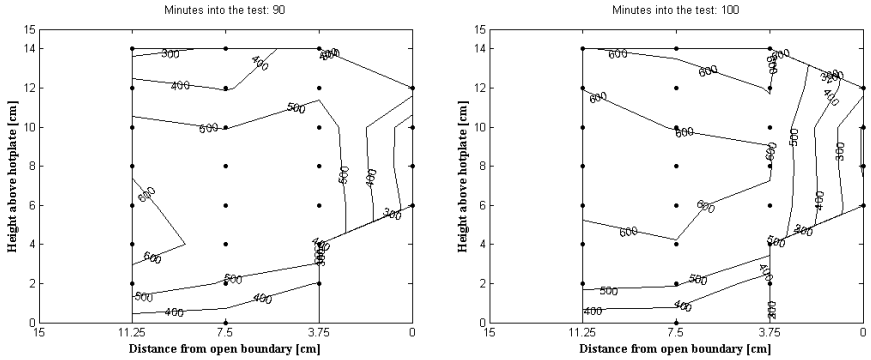

a) Temperatures at 90 min **b) Temperatures at 100 min**

Figure 4.8: Temperature contour plot of a pure smoldering case with density 60 kg/m^3 and open boundary. Part a) shows the temperature in plane A (see figure 3.5) at 90 minutes, 10 minutes earlier than shown in figure 4.6a and 4.6b. The plot shows a more homogeneous combustion spatially than in figure 4.6a and 4.6b. Part b) shows the temperature in plane A (see figure 3.5) at 100 minutes. Here all the cotton has a temperature higher than the temperature for onset of smoldering and the whole sample is smoldering. The temperatures at the boundary are affected by cold ambient air, with lower temperatures than expected for smoldering. The thermocouples are indicated by dots.

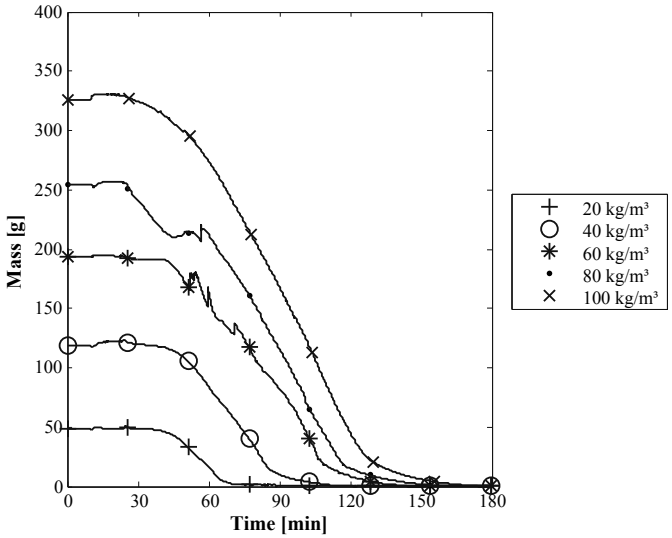

Figure 4.9: Sample mass as a function of time for different densities during smoldering, using scenario A.

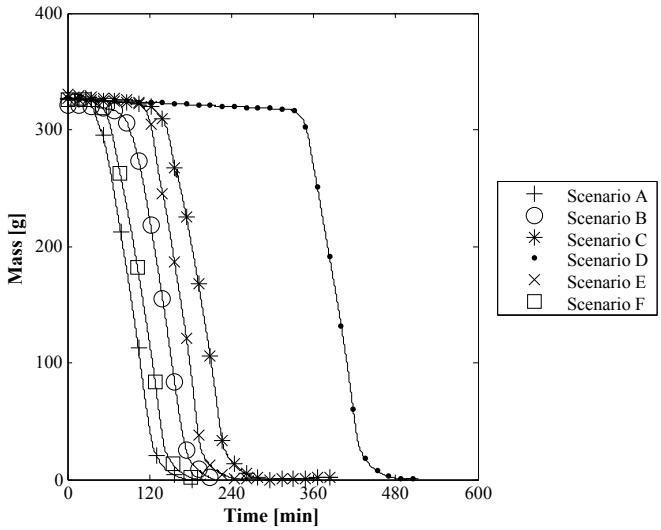

Figure 4.10: Sample mass as a function of time for density 100 kg/m^3 during smoldering, using all six scenarios.

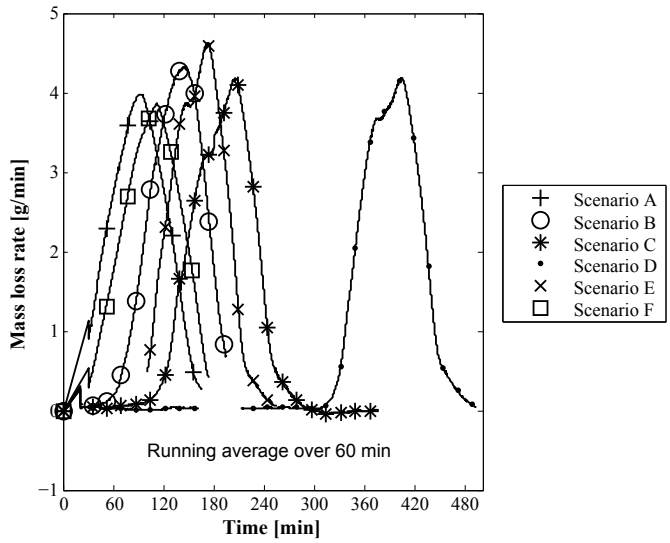

Figure 4.11: Mass loss rate as a function of time with density 100 kg/m^3 for all scenarios. The time interval where mass loss occurs is affected by the heat flux scenario, but the functional form is similar for the six scenarios.

loss rate is given in table 4.5 and figure 4.12. The average mass loss rate increases from 2 to 3.5 g/min as the density increases from 20 to 100 kg/m^3. In figure 4.13 mass and time for scenario A are scaled with initial mass (m_o) and total time it takes to consume the cotton (t_{end}). With this simple rescaling, the curves for different densities are reasonably close. Note that the remaining variability is systematic with density: the higher the density, the further to the left is the curve. Furthermore, the effect of density is diminishing as the density increases, as is consistent with decreased permeability and oxygen transport into the sample and reduced convection within the cotton.

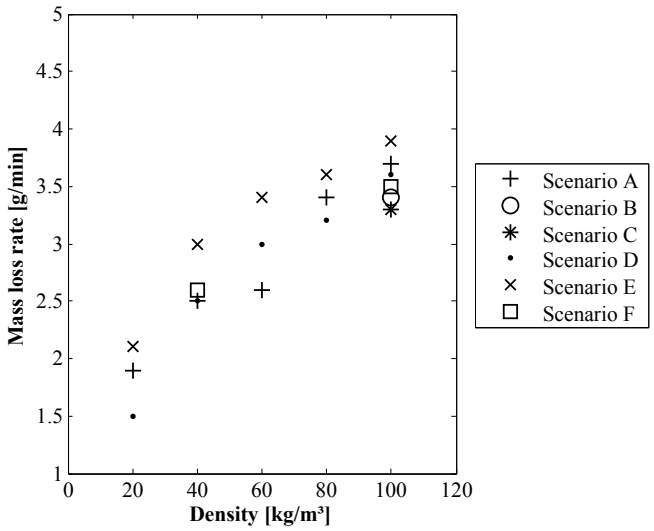

Figure 4.12: Average mass loss rate as a function of density for all six heat flux scenarios.

4.4.2 Mass loss rate as a function of boundary

Mass loss rate as a function of time with a lightweight concrete boundary, is shown in figure 4.14, while the average mass loss rate is shown in table 4.6. The flaming case differs significantly from the non-flaming (pure smoldering) cases. Three observations can be made from figure 4.14. Before flaming, the mass loss rate is similar for both flaming and non-flaming cases. After the transition to flaming, the mass loss rate for the flaming case exceeds the non-flaming case. This is consistent with an increased mass loss due to radiation from the flame. Finally, when the flames are extinguished the mass loss rate for the flaming case is lower than for the non-flaming cases. This is consistent with the flames consuming most of the sample, leaving little material for the subsequent smoldering phase.

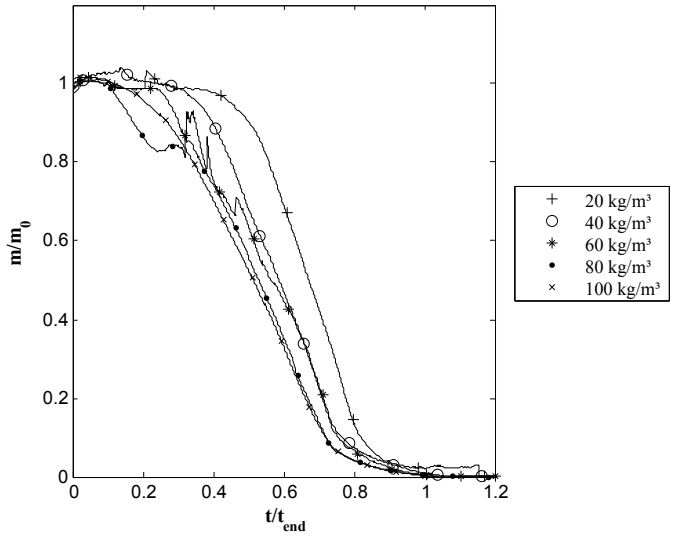

Figure 4.13: Mass (m) scaled by start mass (m_0) as a function of time (t) scaled by the time it takes to consume the cotton (t_{end}) for scenario A. Mass loss and time is from the cases figure 4.9.

Table 4.5: Average mass loss rate for pure smoldering cotton as function of density and heat flux scenario.

	Scenario					
	A High heat flux followed by cooling	B Medium high heat flux followed by cooling	C Medium low heat flux followed by cooling	D Low constant heat flux	E High heat flux followed by low constant heat flux	F Multiple heating and cooling of the same sample
Density (kg/m^3)	(g/min)	(g/min)	(g/min)	(g/min)	(g/min)	(g/min)
5.5	*	-	-	-	-	-
20	1.9	-	-	1.5	2.1	-
40	2.5	-	-	2.5	3.0	2.6
60	2.6	-	-	3.0	3.4	-
80	3.4	-	-	3.2	3.6	-
100	3.7	3.4	3.3	3.6	3.9	3.5

* No ignition
- Not investigated

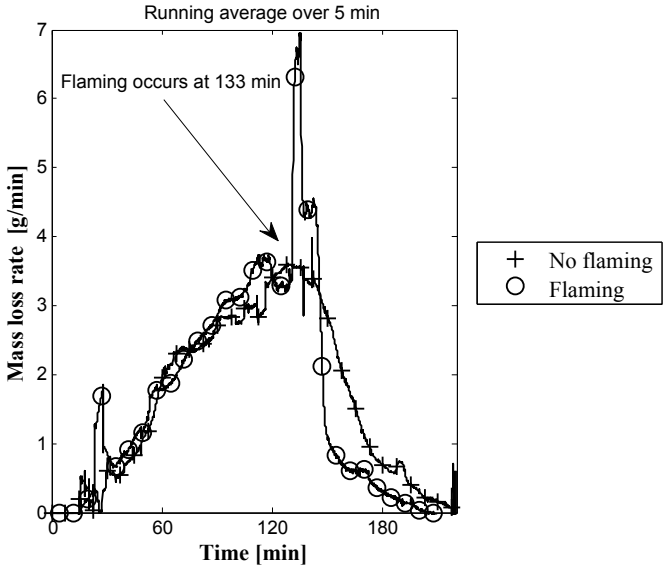

Figure 4.14: Mass loss rate as a function of time for cotton with density 100 kg/m^3 for a case with a lightweight concrete block at the boundary. For the non-flaming results (pure smoldering cases) the mass loss rate is the average over four experiments. During flaming the mass loss rate increases compared with the smoldering case.

Table 4.6: Average mass loss rate as a function of density and boundary condition. The average mass loss rate is based on the mass reduction from 90 to 10% of the initial value. The values for open boundary and flaming cases are calculated from one experiment, while for non-flaming the numbers of experiments the average is made from, are given in a parenthesis.

	Boundaries		
Density	Open	Lightweight concrete block	
		Non-flaming	Flaming
(kg/m^3)	(g/min)	(g/min)	(g/min)
20	1.6	$\pm$ 0.2 (5 tests)	-
60	2.7	2.5 $\pm$ 0.1 (2 tests)	na.
80	2.8	2.7 $\pm$ 0.2 (3 tests)	3.3
100	3.1	2.9 $\pm$ 0.2 (4 tests)	2.9
* No ignition		na. Not available	
- Not investigated			

4.5 Smoldering velocity

4.5.1 Smoldering velocity as a function of density and scenario

The speed at which the smoldering reaction front moves through the sample at the vertical centerline is shown in figures 4.15, 4.16 and table 4.7. The results are for non-flaming cases with heat flux scenarios A to F. The velocity is found using the estimated ignition temperature for each density and scenario (see table 4.1) as an indicator for when the smoldering reaction front reached a thermocouple. This allows calculation of an average velocity between two thermocouples. The average smoldering velocity shown in table 4.7 varies between 1.5 and 5.5 mm/min, which is in good agreement with the 3 mm/min reported by Ohlemiller and Roger [64]. Density affects the smoldering velocity; low density results in high smoldering velocities, while high density results in lower velocities. The effect of the heat flux scenarios on the average smoldering velocity is minor. A general trend is that the smoldering velocity increases as the smoldering front moves through the sample (see figure 4.15 and 4.16). The results in figure 4.16 show a doubling in smoldering velocity as the smoldering front moves from 2 to 14 cm above the hotplate. Similar trends have been reported by Torero and Fernandez-Pello for polyurethane foam [79].

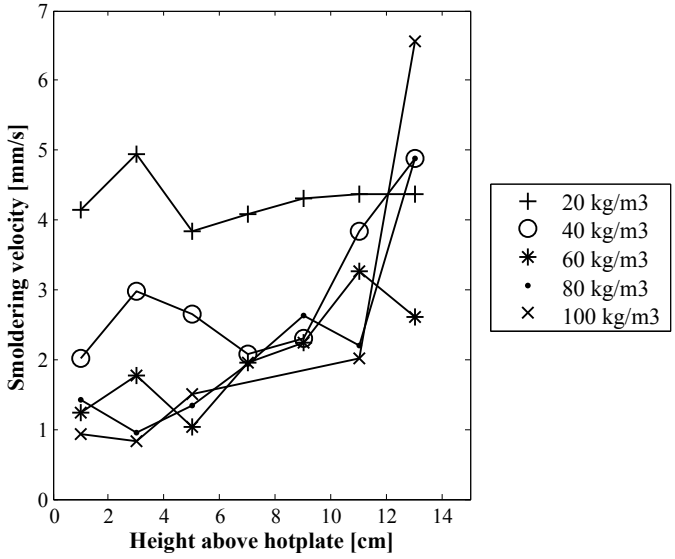

Figure 4.15: Smoldering velocity as function of height above hotplate. The velocities are for scenario A and different densities.

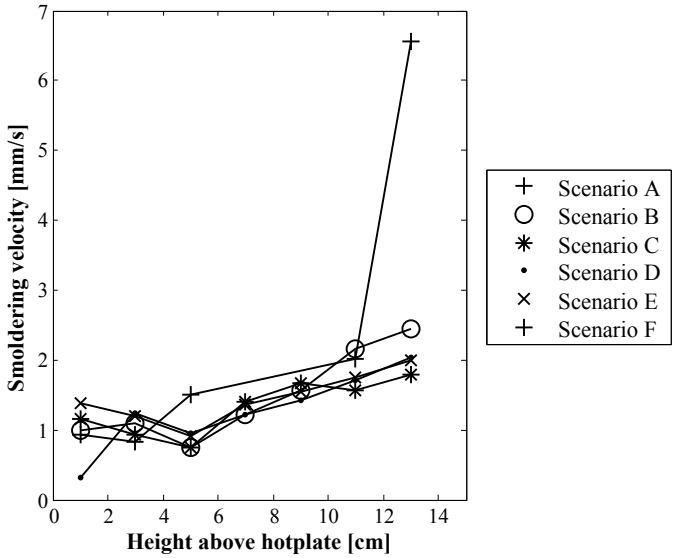

Figure 4.16: Smoldering velocity as function of height above the hotplate for different heating scenarios. For all cases, the sample density was 100 kg/m^3.

Table 4.7: Average smoldering velocity along the vertical centerline as a function of density and scenario.

	Scenario					
	A High heat flux followed by cooling	B Medium high heat flux followed by cooling	C Medium low heat flux followed by cooling	D Low constant heat flux	E High heat flux followed by low constant heat flux	F Multiple heating and cooling of the same sample
Density (kg/m^3)	(mm/min)	(mm/min)	(mm/min)	(mm/min)	(mm/min)	(mm/min)
5.5	*	-	-	-	-	-
20	4.2	-	-	4.0	5.5	-
40	3.0	-	-	5.3	2.9	3.1
60	2.0	-	-	2.1	2.1	-
80	2.2	-	-	1.6	1.7	-
100	2.3	1.5	1.3	1.3	1.5	2.1

* No ignition
- Not investigated

4.5.2 Smoldering velocity as a function of boundary

Table 4.8 gives the average smoldering velocities along the centerline with different boundary. The average smoldering velocity along the vertical centerline of the sample is not affected by the boundary condition. However, considering velocities in different sections of the sample, effects of boundaries appear. In figure 4.17 the temperature as a function of time is shown along four vertical lines in plane A (see figure 3.5b). Figures 4.17a-d show that the time for the smoldering front to reach the top of the sample is longer closer to the lightweight concrete block. Moving from the open side of the sample towards the block, the time at which there is a sudden increase in the temperature at height 12 cm (indicated by arrows) increases from 95 min in part (a) to 102 min in part (b), 107 min in part (c) and 114 in part (d). Flames occurred at 118 min. The same tendency is reflected in figure 4.18c where the time to reach the temperature for onset of smoldering (ca. 309 °C for cotton with density 80 kg/m^3, see table 4.4) is shorter for the thermocouples located away from the block.

Table 4.8: Average smoldering velocity along the vertical centerline. The values for open boundary and flaming are each from one experiment, while for non-flaming the numbers of experiments the average value is based on is given in parenthesis.

	Boundaries		
Density (kg/m^3)	Open	Light weight concrete block	
		Non-flaming	Flaming
	(mm/min)	(mm/min)	(mm/min)
20	4.0	4.4 $\pm$ 0.5 (5 tests)	-
60	2.1	1.9 $\pm$ 0.1 (2 tests)	1.8
80	1.5	1.5 $\pm$ 0.1 (3 tests)	1.4
100	1.3	1.2 $\pm$ 0.1 (3 tests)	1.5
* To be tested			
na - not available			

The temperature distribution in the samples not leading to flaming is more homogeneous compared with the experiments where flaming occurred. In figure 4.18 the time to reach the temperature for onset of smoldering as a function of height is shown. The temperature distribution in the case of transition to flaming fire (figure 4.18c), differs from the other cases. For the non-flaming cases (figure 4.18a and 4.18b) the time to reach the temperature for onset of smoldering does not vary within a layer. For the flaming case (figure 4.18c) the time is longer closer to the block of lightweight concrete. This difference makes the formation of the region with warm un-combusted cotton possible.

In figure 4.19 the smoldering velocity for the case in figure 4.17, is shown. There are significant differences in the velocity with position in the sample. Between 6 and 8 cm from the hotplate, the smoldering velocity is approximately the same for the whole sample. However,

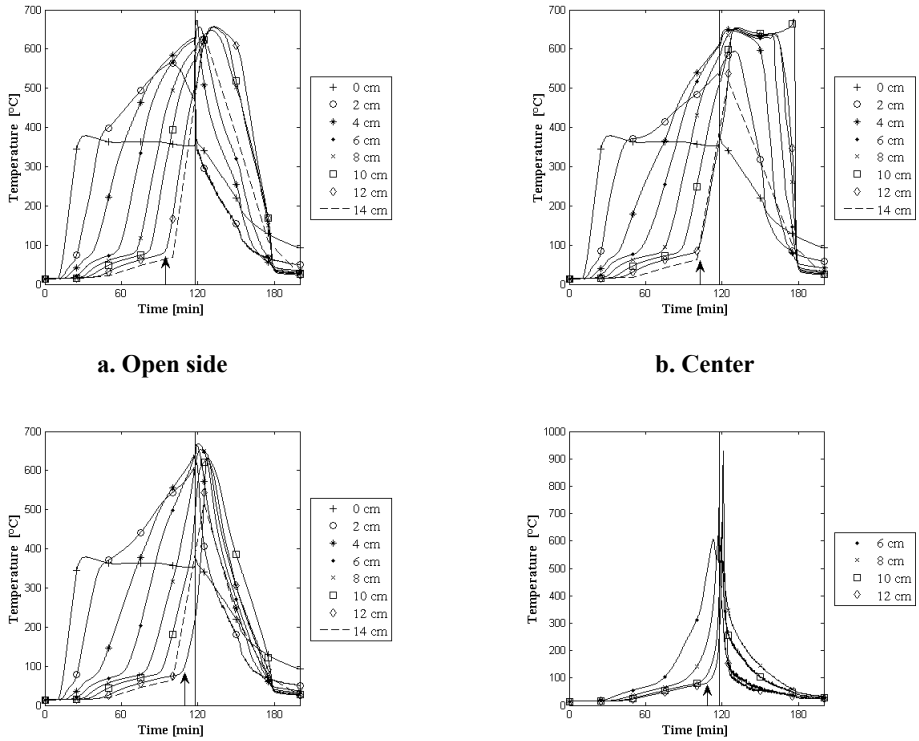

a. Open side **b. Center**

c. Towards block **d. Next to block**

Figure 4.17: Temperature as a function of time for cotton with density 80 kg/m^3 and lightweight concrete boundary. Flames occured at 118 min, as indicated by the vertical line in the plot. In part (a) the temperatures at the vertical centerline in plane A 11.25 cm from the lightweight concrete block are shown. The heights are above the level of the hotplate, as shown in the legends. Parts (b) and (c) show the temperatures 7.5 cm and 3.75 cm from the block, while part (d) shows the temperatures at the boundary between the cotton and the lightweight concrete block. In part (d), the temperature exceeds 900 °C as the flames move through the sample. Note that the temperature scale in part (d) is extended to account for the higher temperatures due to flaming.

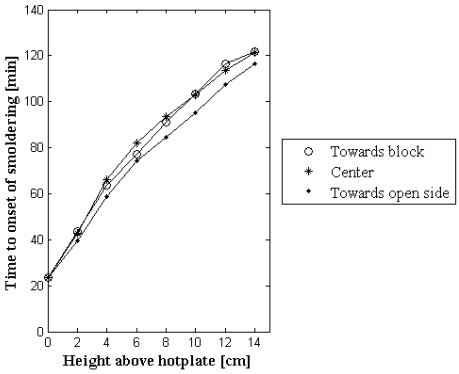

a) Open boundaries

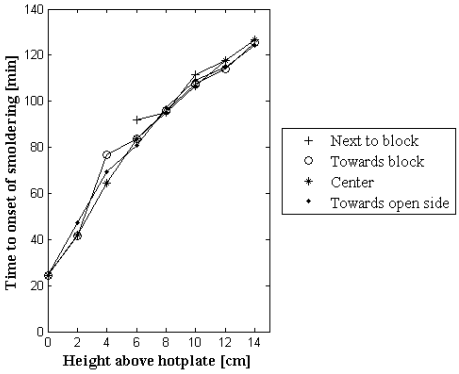

b) One boundary covered by a concrete block – no flaming

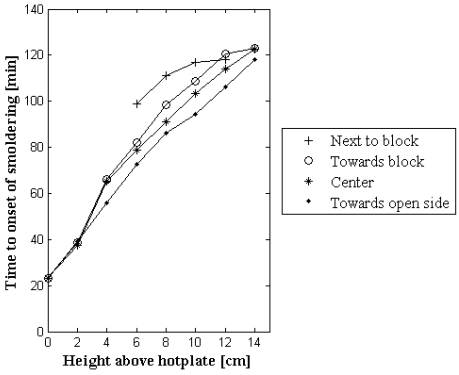

c) One boundary covered by a concrete block – flaming

Figure 4.18: Time to onset of smoldering at different locations in the sample as a function of height above hotplate. The data in (c) is extracted from the temperature measurements shown in figure 4.17. The cotton had density 80 kg/m^3. Time to onset of smoldering is higher closer to the block of lightweight concrete.

between 8 and 12 cm both the velocities "next to" and "towards the block" are significantly higher. This is consistent with formation of char in the sample, and a better transport of oxygen into the sample leading to secondary char oxidation and flaming. The high smoldering velocities in figure 4.19 "next to" and "towards the block" occur as the flames move through the sample. Both figure 4.18 and 4.19 indicate the presence of a region of warm un-combusted cotton near the lightweight concrete block.

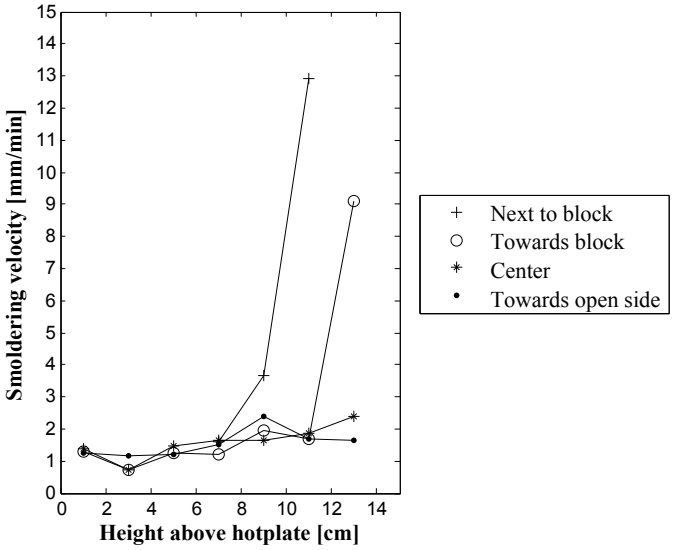

Figure 4.19: Smoldering velocity as a function of height above the hotplate, with cotton density 80 kg/m^3. The temperature distribution is shown in figure 4.17. The average velocity between pairs of thermocouples is shown. The smoldering velocity is higher closer to the block of lightweight concrete in the upper parts of the sample, as a result of a short period of flaming.

Chapter 5

Modeling of ignition temperature

Ohlemiller's ignition model (described in section 2.3.2) is based on a stationary situation with time independent temperatures through a thin sample [55]. By assuming a stationary situation, and using material parameters such as conduction, convection, sample thickness and ambient temperature, Ohlemiller could estimate the ignition temperature for a thin one-dimensional sample. The samples used in the present work are not thin and Ohlemiller's model must be extended in order to incorporate semi-infinite materials.

5.1 Modeling of onset of smoldering

Ohlemiller's model is based on balance between heat production and heat loss [55],

$$\Delta H_c \rho l_R A^* e^{\frac{-E_a}{RT_P}} = \frac{k}{l}(T_P - T_a), \tag{5.1}$$

where ΔH_c is heat of combustion, ρ is density, A^* is a pre-exponential factor, E_a is the activation energy, R is the gas constant, T_P is the hotplate temperature, T_a is the ambient temperature, l is the characteristic length and l_R is the thickness of the reaction zone. If the heat production exceeds the heat loss, smoldering will occur. The heat transfer within a porous material consists of conduction, convection and radiation [74]. Tye [83] gives a thermal conductivity coefficient, that includes effects of different heat transfer modes present in cellulose. In the present article, heat transfer will be calculated using Fourier's law [33] with Tye's thermal conductivity coefficient [83]. Material properties are listed in table 5.1.

The balance in eq. 5.1 is dependent on how far the heat has spread in a sample. This is described through a heat loss zone with characteristic length l. Two models with different approaches to the heat loss zone are developed below.

Table 5.1: Material properties for cotton

Property	Reference
$A = 1 \cdot 10^5$ s^{-1}	[34]
$E = 102 \cdot 10^3$ J mol^{-1}	[35]
$h = 10$ W m^{-2} K^{-1}	[33]
$k_{(\rho=5.5)} = 0.036$ Wm^{-1} K^{-1}	Extrapolations based
$k_{(\rho=20)} = 0.038$ Wm^{-1} K^{-1}	on values
$k_{(\rho=40)} = 0.039$ Wm^{-1} K^{-1}	from Tye [83]
$k_{(\rho=60)} = 0.041$ Wm^{-1} K^{-1}	
$k_{(\rho=80)} = 0.043$ Wm^{-1} K^{-1}	
$k_{(\rho=100)} = 0.044$ Wm^{-1} K^{-1}	
$\Delta Hc = 17.3 \cdot 10^6$ J kg^{-1}	[34]
$R = 8.31431$ J K^{-1} mol^{-1}	
$T_a = 293$ K	
$\rho = 5.5 - 100$ kg m^{-3}	

5.1.1 Heat loss zone with constant thickness

As described in section 2.3.2, Ohlemiller's model is based on a thin sample, where the back of the sample is a free surface cooled by convection. As a first approach to model the temperature for onset of smoldering for the current experimental setup, the characteristic length (l) of the heat loss zone is assumed to be constant. In order to use Ohlemiller's theory it is also assumed that the sample is cooled by convection above the heat loss zone.

From experimental results for scenario A, in figure 5.1, the most significant temperature reduction in the cotton occurs between the hotplate and the sample height of 0.04 m. For cotton with density 20 kg/m^3, the temperature reduction is most significant between the hotplate and 0.08 m. The characteristic length (l) is therefore set to 0.04 m, even though this is somewhat short for the cotton with density 20 kg/m^3.

In Ohlemiller's model the temperature gradient (b) is calculated using conduction (k) and convection factors (h), sample thickness (l), hotplate temperature (T_P) and ambient temperature (T_a), assuming a stationary situation [55],

$$b = (T_P - T_a)\frac{h}{k}\left(\frac{1}{1+(hl/k)}\right). \tag{5.2}$$

In the current experiments the material is not thin and the temperature gradient is established by assuming that the length of the heat loss zone replaces the thickness of the sample. The characteristic length (l) is therefore set to 0.04 m. The temperature gradient (b) in the sample can then be estimated using equation 5.2.

The temperature gradient is used to estimate the thickness of the reaction zone (l_R) in the

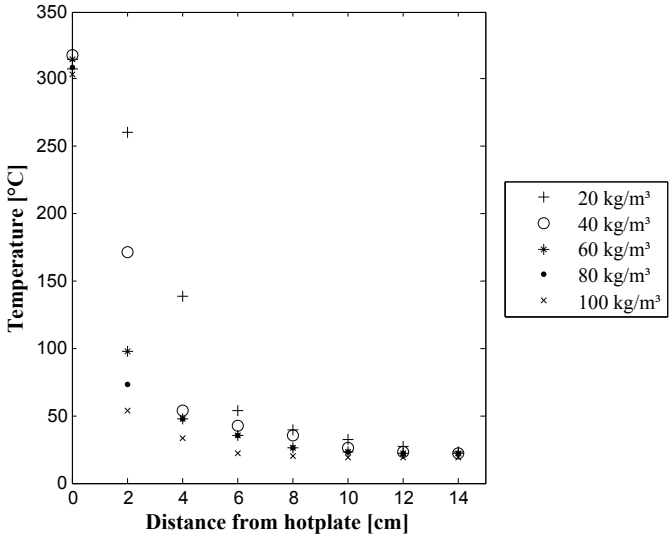

Figure 5.1: Temperature profile within the cotton sample at the estimated ignition temperature. At ignition, most of the temperature reduction is between the hotplate and the third thermocouple (0.04 m) where the temperature is around 50 °C. As discussed in the text, a reasonable estimate for the characteristic length (l) in eq. 5.1 and 2.13 is therefore 0.04 m. The exception is cotton at 20 kg/m^3, where most of the temperature reduction occurres between the hotplate and 0.08 m.

sample using [55]

$$l_R = \frac{RT_p^2}{bE_a}. \tag{5.3}$$

The temperature for onset of smoldering (T_P) is estimated numerically using eq. 5.1. The calculated temperature for onset of smoldering fire for scenario A, is shown in table 5.2. For scenario A, using a constant heat loss zone, the temperature for onset of smoldering in cotton can be estimated to within $\pm 2\%$ of the experimental values. However, for other heat flux scenarios, a constant heat loss zone of 0.04 m underestimates the temperature for onset of smoldering. The model also uses convection at the surface where the heat loss zone ends, which does not reflect the heat transport higher in the sample. For thermally thick materials the heat loss zone will be affected by a combination of conduction, convection and radiation.

Table 5.2: Estimated temperatures for onset of smoldering as function of density and constant heat loss zone of 0.04 m for scenario A.

Density (kg/m^3)	Experimental results A for onset of smoldering (°C)	Calculated ignition temperatures (°C)	Error (%)
5.5	*		
20	307 ± 2	320	2
40	318 ± 3	319	0
60	315 ± 2	309	-1
80	309 ± 2	301	-1
100	303 ± 2	295	-1
* No ignition			

5.1.2 Temperature-determined heat loss zone

A constant characteristic length (l) as obtained above leads to estimated values that deviate from the experimental ones (see table 5.2) . An alternative way to determine the characteristic length (l) is to use an effective layer depth to find the temperature gradient (b) through the material. The effective depth is defined as the distance from the hotplate to the level where the temperature is 40 °C, which will be referred to as the limiting temperature, T_{lim}. The temperature increase between 40 and 80 °C is affected by evaporation of water (see section 4.1). Different values for the limiting temperature have been investigated as described in section B.1. T_{lim} = 40 °C was found to give the best overall estimate of the ignition temperature. Thus,

$$b = \frac{(T_P - T_{lim})}{l}. \tag{5.4}$$

The effective depth (l) is found from experimental data, by interpolating between the heights of the thermocouples that are above and below the limiting temperature. When the

effective length is found, the depth of the reaction zone is calculated using eq. 5.3 and 5.4. Table 5.3 gives the effective depth (l) and the thickness of the reaction zone (l_R) for scenarios A, D and E. Ohlemiller [55] reports a reaction zone for cellulose of 0.004 m. Scenario A shows similar values as reported by Ohlemiller, while the reaction zones for scenarios D and E are thicker.

Near the onset of smoldering, the heat loss is assumed to be equal to the heat generation and the ignition temperature (T_P) can be found using

$$\Delta H_c \rho l_R A^* e^{(-E_a/RT_P)} = \frac{k}{l}(T_P - T_{lim}). \tag{5.5}$$

Where T_{lim} has been inserted for T_a as compared with eq. 5.1. Material properties are listed in table 5.1. Ignition temperatures for different densities and scenarios are listed in table 5.4. The model estimates the ignition temperature for scenario A to within 1-3% of the experimental results, while the deviation for scenarios D and E is approximately 2-7%. The model with a temperature-determined heat loss zone reproduces the reduction in ignition temperature with increasing density, but underestimates systematically the ignition temperature.

5.2 Transient modeling of onset of smoldering

The ignition model with the temperature-determined heat loss zone developed in section 5.1.2, will be combined with a one-dimensional numerical heat transfer model to estimate the time to and temperature at onset of smoldering. The one-dimensional heat transfer model is the numerical solution of the heat transfer equation [25],

$$\rho c \frac{\partial T}{\partial \tau} = k \frac{\partial^2 T}{\partial z^2} + \dot{Q}. \tag{5.6}$$

The numerical solution of eq. 5.6 is [33]

$$T_m^{p+1} = \frac{\alpha \Delta \tau}{(\Delta z)^2}(T_{m+1}^p + T_{m-1}^p) + \left[1 - \frac{2\alpha \Delta \tau}{(\Delta z)^2}\right] T_m^{p+1} + \dot{q}''' \Delta z \Delta \alpha \Delta \tau / k, \tag{5.7}$$

where T_m^p is the temperature at node m at time step p, $T_m^{p+1}$is the temperature at node m at the following time step (p+1), T_{m+1}^p and T_{m-1}^p are the temperatures at the surrounding nodes m+1 and m-1, α is the thermal diffusivity, $\Delta\tau$ is the time step and Δz is the distance between nodes. $\dot{Q}$ is the energy production. Based on an Arrhenius approximation, the energy production pr. volume, $\dot{q}'''$, is [86]

$$\dot{q}''' = \Delta H_c \rho A^* e^{(-E_a/RT_P)}. \tag{5.8}$$

Information on temperature-dependent material properties for cotton with absorbed water

Table 5.3: Effective depth (l) and reaction layer thickness (l_R) for a temperature-determined heat loss zone.

	High heat flux followed by cooling		Low constant heat flux		High heat flux followed by low constant heat flux	
Scenario	A		D		E	
Density (kg/m^3)	Effective depth (l) (m)	Reaction layer thickness (l_R) (m)	Effective depth (l) (m)	Reaction layer thickness (l_R) (m)	Effective depth (l) (m)	Reaction layer thickness (l_R) (m)
20	0.08	0.008	0.11	0.011	0.12	0.012
40	0.07	0.007	0.10	0.010	0.08	0.009
60	0.05	0.005	0.09	0.010	0.08	0.009
80	0.05	0.005	0.08	0.009	0.08	0.008
100	0.03	0.003	0.07	0.007	0.07	0.007

Table 5.4: Experimental ignition temperatures and estimated temperatures for onset of smoldering with a temperature-determined heat loss zone.

	High heat flux followed by cooling			Low constant heat flux			High heat flux followed by low constant heat flux		
Scenario	A			D			E		
Density (kg/m^3)	Experimental ignition temperature (°C)	Estimated ignition temperature (°C)	Deviation (%)	Experimental ignition temperature (°C)	Estimated ignition temperature (°C)	Deviation (%)	Experimental ignition temperature (°C)	Estimated ignition temperature (°C)	Deviation (%)
20	307 ± 2	314	1	306 ± 4	295	-2	336 ± 4	291	-7
40	318 ± 3	304	-2	320 ± 6	283	-6	302 ± 7	290	-2
60	315 ± 2	308	-1	319 ± 7	274	-7	305 ± 10	279	-4
80	309 ± 2	299	-2	305 ± 5	273	-5	300 ± 10	276	-4
100	303 ± 2	320	3	284 ± 5	275	-2	303 ± 11	279	-4

is scarce. Approximate values are obtained by combining values for dry cotton and water. There is approximately 5% moisture by weight in the cotton (see section 4.1) that affects (apparent) conductivity and specific heat. The temperature-dependent conductivity of cotton is calculated using

$$k = 0.95 \cdot k_{cotton} + 0.05 \cdot k_{moisture}, \tag{5.9}$$

where k_{cotton} and $k_{moisture}$ are given in table 5.5. The conductivity of dry cotton (k_{cotton}) is assumed to be constant as function of temperature, but dependent on density (see table 5.1) [83]. In table 5.5 properties for water at three different temperature regions are given. It is assumed that moisture evaporates at a constant rate between 40 and 80 °C (see section 3.1 and 4.1) and that its effects on conductivity and specific heat are reduced systematically with increasing temperature.

Table 5.5: Material properties for cotton with density 100 kg/m^3.

Dry cotton		
Conductivity	k_{cotton} = 0. 044 W/(m K)	
Spesific heat	$c_{p,cotton}$ = (1075+4.27·(T[K]-293)) J/(kg K)	
Water		
Temperature region	Conductivity W/(m K)	Specific heat J/(kg K)
T< 313 K	$k_{moisture}$ = 0.62	$c_{p,moisture}$ = 4180
313K $\leq$ T < 353 K	$k_{moisture}$ = 0.62-0.0155·(T[K]-313)	$c_{p,moisture}$ = 61904
353 K $\leq$ T	$k_{moisture}$ = 0	$c_{p,moisture}$ = 0

The specific heat of dry cotton increases linearly with temperature as reported by Hatakeyama et al. [31]. These results were reported to be valid only from 50 °C, due to effects of moisture. Here the results of Hatakeyama et al. will be used from 20 °C, since the effect of water absorbed in the cotton will be treated separately. The temperature-dependent specific heat of dry cotton is [31]

$$c_{p,cotton} = (1075 + 4.27 \cdot (T[K] - 293)) \frac{J}{(kgK)}. \tag{5.10}$$

The apparent specific heat for absorbed water results from both heating and vaporization. An approximation for the specific heat of the moisture within the cotton is (see table 5.5)

$$c_{p,moisture} = \frac{\text{Enthaply}}{\text{Temperature}} = \frac{\Delta h}{\Delta T}. \tag{5.11}$$

Water heated from room temperature to 40 °C [7]

$$c_{p,\,moisture20-40°C} = \frac{167.55 - 83.96}{20} \cdot 10^3 \frac{J}{kgK} = 4180 \frac{J}{kgK}. \tag{5.12}$$

Water heated and evaporated between 40 °C to 80 °C [7]

$$c_{p,\,moisture40-80°C} = \frac{2643.7 - 167.55}{40} \cdot 10^3 \frac{J}{kgK} = 61904 \frac{J}{kgK}. \tag{5.13}$$

The resulting values for overall specific heat and conductivity for cotton with absorbed water are illustrated in figure 5.2a and b and in table 5.5. The model used is a heat transfer model, water vapor transport has therefore not been included. By not including water vapor an error of maximum 5% is introduced to k_{cotton} and $C_{p,cotton}$. The density of cotton is also affected by the evaporation of water [22]. In this model it is assumed that the weight is reduced linearly from 100 to 95% of the initial weight when the temperature increases from 40 to 80 °C.

Using the specific heat, conductivity and density as described above, the temperature profile in the cotton sample can be determined as shown in figure 5.3. Using the 1D heat transfer model and the ignition model described in section 5.1.2, the time to and temperature at onset of smoldering were calculated. Scenarios A, D and E with density 100 kg/m^3 have been investigated. As shown in table 5.6 the temperature for onset of smoldering for scenario A is estimated to 312 °C compared with the experimental result of 303 °C, while for scenarios D and E the estimated temperatures are 253 and 290 °C compared with the experimental values of 284 and 303 °C, respectively. The calculated values deviate from the experimental ones by 9 to 31 °C or 2 - 6%. The estimated time to onset of smoldering was also calculated. For scenario A the calculated time is 1766 s while the experimental result is 1538 s, - a deviation of 24%. For scenarios D and E the deviations are about 30-50 %.

The results indicate that the one-dimensional approach can be used for scenarios where the material is thermally thick, and where the time to onset of smoldering is shorter than the time it takes for the heat front to reach the boundaries of the sample. Scenario A with a density of 100 kg/m^3 is one example. In figure 5.3 one notes that the model fits the experimental results for the temperature 2 cm above the hotplate reasonably well up to time 1860 s but deviates significantly later. The current 1D-model does not account for the 3-dimensional heat loss that is important throughout scenarios D and E. To get a more accurate estimate for the time to smoldering, 2- or 3-dimensional heat transfer models must be developed.

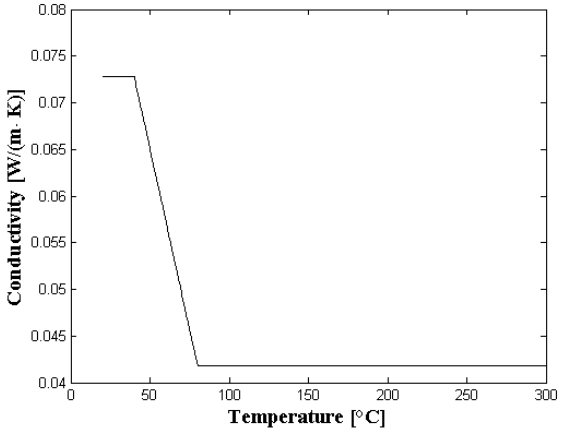

a) Conductivity

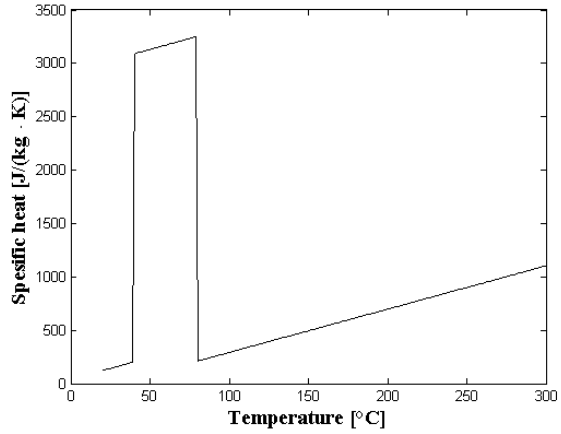

b) Specific heat

Figure 5.2: Illustration of conductivity and specific heat for cotton with density of 100 kg/m^3 containing 5% water by weight as described in table 5.5.

Table 5.6: Estimated time to and temperature at onset of smoldering using 1D-simulation of Scenarios A, D and E with density 100 kg/m^3

	Scenario A		Scenario D		Scenario E	
	Ignition time (s)	Ignition temperature (°C)	Ignition time (s)	Ignition temperature (°C)	Ignition time (s)	Ignition temperature (°C)
Experimental results	1538	303	15360	284	4740	303
Simulation	1766	312	10438	253	2713	290
Deviation	24%	2%	-33%	-6%	-49%	-2%

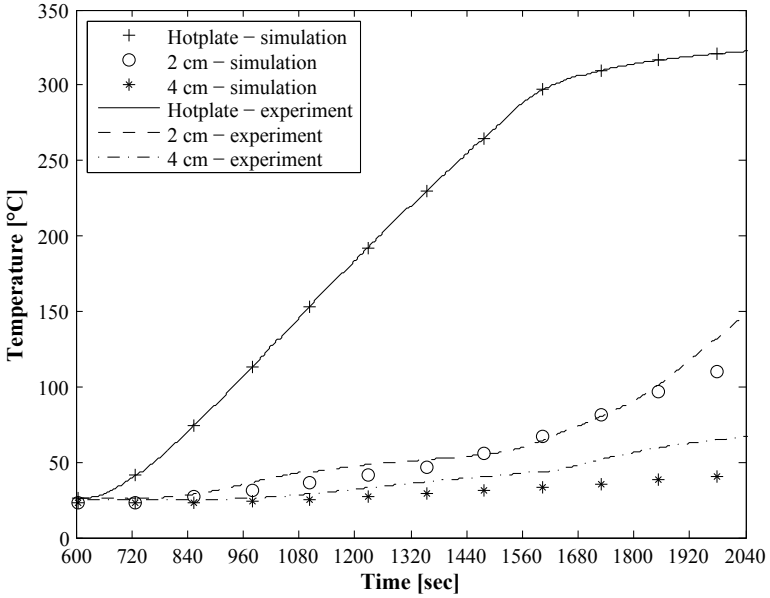

Figure 5.3: Temperatures as a function of time for scenario A with density 100 kg/m^3.

Chapter 6

Discussion

6.1 Onset of smoldering

Onset of smoldering has been investigated using different densities and heat flux scenarios, as shown in table 4.1.

From table 4.1 the effect of density is evident in scenarios A and D, where the temperatures for onset of smoldering are reduced with increasing density. For scenario A the ignition temperature is reduced from 318 to 303 °C as the density is increased from 40 to 100 kg/m^3. The ignition temperature for scenario D is reduced by 36 °C over the same density interval. For scenario E a similar trend is less clear.

Density affects both heat transfer and energy production in cotton. Heat transfer in porous materials is a complex combination of conduction, convection and radiation [53]. An increase in density will reduce the porosity and thereby convection. The increase in conduction due to a denser medium can probably not compensate for the reduced heat transfer due to less convection. Thus, the heat transport within the cotton will be slowed down. The energy from the hotplate will accumulate in a hot layer, instead of being transported away. The energy production in the hot layer is affected by the density, as described by eq. 2.11. The combined effects of increased density on heat transfer and heat production lead to a buildup of a hot decomposing layer and onset of smoldering combustion at lower temperatures as density increases. Since density affects heat transfer and heat production, it should be included when defining standards for material testing.

The results in table 4.1 for density 100 kg/m^3 show that the heating scenario affects the ignition temperature. Scenario D, with a low constant heat flux, has a significant lower ignition temperature compared with the other scenarios. Figure 6.1 shows the temperature profile at ignition for different scenarios. The temperature profile for scenario D shows a layer with increased temperatures higher into the cotton. The balance between energy production and heat

transfer within this layer causes onset of smoldering at a lower temperature than for other scenarios. The time to ignition with scenario D is significantly longer than for the other scenarios, see table 4.1.

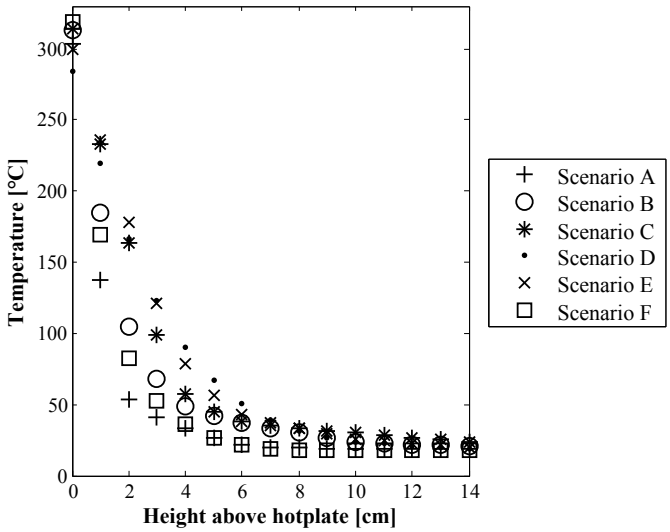

Figure 6.1: Measured temperature profiles at ignition for density 100 kg/m^3 with different heating scenarios. For scenario D the heat has spread higher up through the cotton compared with the other scenarios.

The significant difference in ignition temperature between scenarios A and D at 100 kg/m^3 motivated experiments with heat flux between 12.8 and 1.5 kW/m^2. Scenarios B and C are similar to scenario A, but the heat flux was lower and the time needed to reach the cut-off temperature longer. The hypothesis was that the ignition temperature for scenarios B and C would lie between 303 °C for scenario A and 284 °C for scenario D. However, both scenarios B and C turned out to give higher ignition temperatures. Compared with scenario A, scenarios B and C are expected to have higher (integrated) heat loss where heat loss through the open boundaries affect the results. Consequently, both the time and temperature necessary to establish a deep enough pyrolysing layer will increase, and a higher ignition temperature is reasonable. Furthermore, in contrast to scenario D, scenarios B and C have a finite time with heat flux from the hotplate. This must be compensated for by heating to a higher temperature. Thus, in order to establish a pyrolysing layer for scenarios B and C, it is reasonable that one needs to reach a higher temperature than for scenarios A and D. Heating scenarios affect the ignition temperature and it must be emphasized that measured ignition temperatures are apparatus dependent. The use of other ignition sources, sample sizes or geometries, could result in different ignition temperatures [55].

Density affects the mass loss rate of smoldering cotton, but the dependency is not linear:

a fivefold increase in density resulted in an approximate twofold increase in the average mass loss rate, as can be seen in table 4.5. In a denser sample, oxygen transportation will be slower, and smoldering reaction rate and heat production reduced. Similar observations are reported by Ohlemiller [60] and Palmer [66]. The mass loss rate is not significantly affected by the heat flux scenarios. This is reasonable, since the scenarios merely represent different routes to the onset of smoldering. The smoldering process as such, on the other hand, is self-driven and regulated through density and geometry of the sample.

The smoldering velocity is only slightly affected by sample density. Lower densities have higher smoldering velocities, as the density increases the velocity decreases. The effect of heat flux scenario is also minor. For sample density 100 kg/m^3 the low heat flux scenarios C, D and E tend to give lower smoldering velocities than high heat flux scenarios (see table 4.7). This could be a result of the continual heating where lighter components in the cotton are released and transported away from the smoldering front, leaving heavier components which are more difficult to ignite and combust.

Smoldering was observed in cotton for densities between 20 and 100 kg/m^3, which corresponds to porosities between 93 and 98%. Cotton with density 5.5 kg/m^3 and porosity 99.6 % was also investigated, but self-propagating smoldering was not observed for this density. Thus, porosity between 98 and 99 % seems to be an upper bound for smoldering in cotton with the present experimental set-up.

Both density and heat flux influence the temperature for onset of smoldering in cotton. The effects are significant, thus, both density and heat flux should be included as parameters in standard tests for determining ignition temperatures for dusts and other cellulose-based materials.

6.2 Transition from smoldering to flaming fire

Transition from smoldering to flaming fire has been investigated with two boundary conditions and for different densities (see table 4.3). Transition to flaming has only been observed for cases where a lightweight concrete block covered one side of the cotton. Furthermore, transition has been observed in cases with densities 60, 80 and 100 kg/m^3, but not for 20 kg/m^3. The transition from smoldering to flaming fire represents a shift from a surface reaction to a gas-phased combustion and requires the presence of sufficient gaseous fuel, oxygen and an ignition source [61].

In figure 4.6a the temperature contour plot for a flaming case is shown 17 minutes before secondary char oxidation and flames occurred. As the smoldering front moved up through the cotton sample, it moved more rapidly along the outer layers of the sample than in the center and next to the lightweight concrete block. Due to the different speeds of the smoldering front,

a region of warm uncombusted cotton was formed next to the lightweight concrete block.

Onset of smoldering in cotton occurs at 280-340 °C (see table 4.1), and the temperature in the region with warm uncombusted cotton is lower. Figure 4.5 shows that the outer layers of the cotton cube have been consumed by smoldering combustion, while the inner part of the sample has not (see figure 4.6a). The region with warm uncombusted cotton has been present in all cases leading to transition. When the smoldering front consumes the region of warm uncombusted cotton, gaseous fuel is generated.

The current experiments show that to get transition to flaming fire, smoldering and secondary char oxidation must coexist. The lightweight concrete block is important to form a region of warm uncombusted cotton, which produces gaseous combustion products. Secondary char oxidation is coupled to the oxygen transport into the char left by the initial smoldering process. When the permeability increases behind the smoldering front, the amount of oxygen transported into the sample increases, resulting in higher heat production and secondary char oxidation [82]. The secondary char oxidation will ignite the gaseous combustion products from the smoldering. Observations during the current experiments show that the transition occured in the char left by the smoldering front. Similar observations have been done by Tse et al. [81]. Since the char is very porous, oxygen will be readily available in this part of the sample.

Secondary char oxidation typically occurs after the smoldering front has reached the top of the sample. There seems to be no correlation between these two events, and glowing has also been observed before the smoldering front reached the top of the sample. The high temperatures in the glowing embers act as an ignition source. When ignition occurred there were several embers in the sample. It is not clear from the current experiments if one ember is energetic enough to cause ignition, or if more embers must be present.

Two boundary conditions have been tested, but only in cases with a lightweight concrete block was transition from smoldering to flaming fire observed. For the scenario with open sides as boundaries there are only small variations in smoldering velocities (see figure 4.18a), thus a region of warm uncombusted cotton is not formed. Without the region of warm uncombusted cotton, the coexistence of the smoldering front and the secondary char oxidation does not occur, and no transition from smoldering to flaming occurs either. Figure 4.18 shows that the temperature distribution in an experiment with transition to flaming fire (figure 4.18c), differs from the other experiments (figure 4.18a and b). For non-flaming cases the time to reach the temperature for onset of smoldering does not vary within a layer. On the other hand, for the flaming case this time is longer closer to the block. This reflects the formation of a region with warm uncombusted cotton.

It is interesting to notice that about 25-50% of the experiments with the lightweight concrete block as the boundary, have transition from smoldering to flaming. The temperature

distribution in the cotton for the non-flaming cases is more homogeneous compared with the experiments where flaming occurred, as shown in figure 4.18a-c. The cases leading to flaming also had a more pronounced tilt of the smoldering fronts compared with the non-flaming cases, as shown in figure 4.3a and b. The time to onset of secondary char oxidation is important for the transition from smoldering to flaming fire. In the cases where transition occurs, the smoldering of the warm uncombusted cotton coexisted with the secondary char oxidation. For the non-flaming cases the secondary char oxidation occurred after the sample was consumed completely by the smoldering front and production of gaseous fuel had ceased. For the case in figure 4.6a the secondary char oxidation occurred at 116 min and flaming occurred at 117 min. For the non-flaming case in figure 4.6b the char oxidation occurred at 144 min, at which all the cotton was consumed by the initial smoldering front.

Flaming was observed for densities: 60, 80 and 100 kg/m^3. For this experimental set-up, 100 kg/m^3 was the maximum density, but the mechanism for transition from smoldering to flaming is probably viable for higher densities. At the lower density (20 kg/m^3) the porosity is high and the transport of oxygen in the cotton sample is less affected by the boundary condition. The smoldering at this density does not leave a region of warm uncombusted cotton that is susceptible for transition from smoldering to flaming fire, similar to the open boundary condition. In one of the experiments secondary char oxidation was observed for density 20 kg/m^3 with the concrete block covering one side. However, the secondary char oxidation occurred after the initial smoldering front had consumed all cotton, and the production of gaseous fuel was negligible. For the other experiments with density 20 kg/m^3 char oxidation was not observed. Observation made of the samples after smoldering had ceased, showed few or no voids in the char left by the smoldering. The lack of voids probably affected the oxygen transport into the char hindering char oxidation. For other densities the presence of voids in the char was significant.

The height of the samples used in these experiments was 0.15 m. The height of the sample was determined from preliminary experiments, where in one case a transition from smoldering to flaming fire was observed (see section 3.2.1). In experiments with higher samples [6, 79], transition to flaming is observed. In small samples density and boundary conditions are important for the coexistence of smoldering and char oxidation.

The results from the current experiments show that smoldering and secondary char oxidation must coexist in a sample in order to get a transition from smoldering to flaming. The coexistence of smoldering and secondary char oxidation for samples with small heights is dependent on both density and boundary conditions. Density and boundary conditions will facilitate different smoldering velocities in a sample, which is important for the coexistence of the smoldering front producing gaseous fuel and secondary char oxidation as the ignition source.

6.3 Modeling the onset of smoldering

A one-dimensional ignition model has been developed (see section 5.1). The model estimates the ignition temperatures to about ± 7 % of the experimental values (see table 5.4). The model uses a characteristic length (l) as the distance from the hotplate to the level where the sample temperature is 40 °C, instead of the entire sample height as described by Ohlemiller [55]. The ignition model is sensitive to the characteristic length.

For scenario A with a density of 100 kg/m^3 the model overestimates the ignition temperature by 32 °C. The characteristic length was extracted from experimental temperature data. The distance of 2 cm between thermocouples, may have been too large to get a good estimation of the characteristic length. Furthermore, the ignition model contains only conduction values as developed by Tye, which do not include moisture **??**. For low density cases like scenario E with density 20 kg/m^3, the underestimated ignition temperature could be a result of convection and radiation not being properly accounted for.

The ignition model has been combined with a one-dimensional heat transfer model to estimate time to and temperature at onset of smoldering combustion. In spite of this relatively crude heat transfer model, these models combined estimate the temperature at onset of smoldering for scenario A at 100 kg/m^3 to within 2% of the experimental value and time to onset of smoldering to within 24% (see table 5.6). The ignition model is based on a one-dimensional semi-infinite slab, while the experimental set-up used is 3-dimensional, freestanding and finite.

The one-dimensional model underestimates both ignition time and temperature for scenarios D and E. Since samples do not behave as semi-infinite slabs in scenarios D and E, 3-dimensional models should be developed for these cases. Sensitivity analysis regarding T_{lim}, number of control volumes and moisture contents is discussed in Appendix B.

The results show that computer modeling of onset of smoldering fire is feasible. However, the models must be further developed in order to account for heat transfer in 3-dimensional samples.

Chapter 7

Conclusions

The ignition temperature for smoldering in cotton has been determined both experimentally and theoretically for several densities and heat flux scenarios. In addition, transition from smoldering to flaming fire has been investigated with regard to effects of boundary conditions and density. The results show that with increasing density, the temperature for onset of smoldering decreases. For a scenario with high heat flux followed by cooling (scenario A) the ignition temperature is reduced from 318 to 303 °C as the density increases from 40 to 100 kg/m^3. At density 100 kg/m^3, a low constant heat flux (scenario D) from a hotplate over 4-5 hours gives a significant lower ignition temperature than a high heat flux over 15-20 minutes and then cooling (scenario A).

Transition from smoldering to flaming occurs in samples where smoldering and secondary char oxidation coexist. For samples with small heights, as used in the current experiments, the smoldering velocity differs with position in the sample due to a boundary of lightweight concrete. As a result of differences in smoldering velocity, a warm uncombusted region forms next to the boundary of lightweight concrete. Secondary char oxidation forming in the char left by the initial smoldering front, ignites gaseous combustion products from the smoldering in the region of warm un-combusted cotton. In samples with low density (20 kg/m^3) or samples with open boundaries, flaming did not occur since the region of warm uncombusted cotton and secondary char oxidation did not coexist.

A one-dimensional ignition model is developed. It estimates the temperature for onset of smoldering to $\pm$ 7 % of the experimental results. The ignition model is combined with a one-dimensional heat transfer model. These models combined estimate the time to and temperature at onset of smoldering for a semi-infinite slab to, respectively, 24% and 2%. More elaborate and three-dimensional numerical models will be needed to estimate the onset of smoldering for more complex geometries and heat flux scenarios.

The current experiments show that boundary conditions and density are important factors for the transition from smoldering to flaming fire. Furthermore, density and heat flux sce-

nario affect the onset of smoldering. The results indicate that density, heat flux and boundary conditions must be included as variables when samples are investigated regarding smoldering.

Chapter 8

Further work

The work in this thesis could be expanded along the following lines:

- The effects of density on different materials:
  The work here has been done on cotton. It would be interesting to investigate if density affects other materials differently regarding onset of smoldering and transition into flaming. A material it would be interesting to test is polyurethane.

- Transition from smoldering to flaming:
  In this work only two boundary conditions have been tested. Further work on how different geometric boundaries affect the transition should be carried out. In addition it would be interesting to see if the materials the boundary consists of affect the transition. In figure 8.1 some geometric boundaries are suggested. Experiments with 80 kg/m^3 in a corner configuration have been carried out. The results in table 8.1 show that 1 of 2 experiments resulted in transition to flaming. The time to transition for the corner configuration was higher compared with the single block.

- Modeling of onset of smoldering:
  In this work 1D-models have been used to estimate the onset of smoldering. It would be interesting to see if 3D-models estimate onset of smoldering better. In addition the heat generation model could be expanded to account for more complex reactions during the decomposition of the fuel.

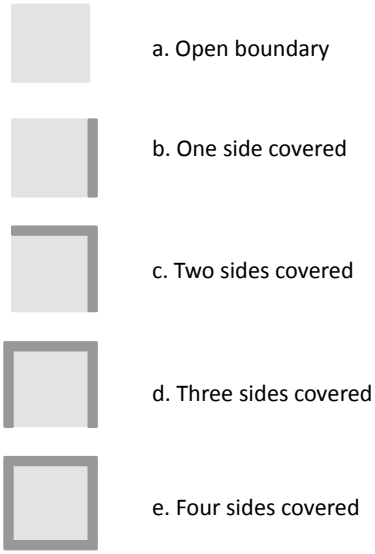

Figure 8.1: Geometry of the boundary, (top view).

Table 8.1: Observed transition from smoldering to flaming as a function of density and boundary. The results for the open boundary and flaming cases are each from one experiment, while the total numbers of experiments with lightweight concrete are given in parentheses. The test with a corner configuration and density 80 kg/m^3 results in flaming.

Density (kg/m^3)	Boundaries				
	Open	Lightweight concrete block			
		With one side covered	With two sides covered	With three sides covered	With four sides covered
20	No	No (5 tests)	*	*	*
60	No	Yes (2 tests) (117 min)	*	*	*
80	No	Yes (3 tests) (118 min)	Yes (2 tests) (130 min)	*	*
100	No	Yes (4 tests) (133 min)	*	*	*

(*) To be tested
( ) Time to transition from smoldering to flaming fire

Appendices

Appendix A

Expression for the energy production

Derivations leading to eq. 2.11 and 2.12 in section 2.3.2 is discussed here [55]. The starting point is eq. 2.10:

$$\int_V \dot{q}'''dV = \int_0^l \Delta H_c \rho A^* \cdot exp\left(-E_a/RT(z)\right)dz. \tag{A.1}$$

It is assumed a linear temperature gradient between S1 and S2, as described in section 2.3.2 and figure 2.7, $T(z) = T_p - bz$,

$$\dot{q}'' = \int_0^l \Delta H_c \rho A^* exp\left(\frac{-E_a}{R(T_p - bz)}\right)dz. \tag{A.2}$$

The expression in eq. A.2 is not solvable analytically. Frank-Kamenetskii's exponential approximation, which involves an expansion to first order, is therefore utilized to solve the expression [78]:

$$\dot{q}'' = \int_0^l \Delta H_c \rho A^* exp\left(\frac{-E_a}{RT_p}\left(1 - \frac{(T_p - bz) - T_p}{T_p}\right)\right)dz, \tag{A.3}$$

$$\dot{q}'' = \Delta H_c \rho A^* exp\left(\frac{-E_a}{RT_p}\right)\int_0^l exp\left(\frac{-E_a bz}{RT_p^2}\right)dz, \tag{A.4}$$

$$\dot{q}'' = \Delta H_c \rho A^* exp\left(\frac{-E_a}{RT_p}\right)\frac{RT_p^2}{E_a b}\left(1 - exp\left(\frac{-E_a bl}{RT_p^2}\right)\right). \tag{A.5}$$

The last part of eq. A.5 is approximately equal to one,

$$\dot{q}'' = \Delta H_c \rho A^* exp\left(\frac{-E_a}{RT_p}\right)\frac{RT_p^2}{E_a b}\left(1 - exp\left(\frac{-102 \cdot 10^3 \text{ Jmol}^{-1}\frac{573 \text{ K} - 273 \text{ K}}{l} l}{8.31431 \text{ JK}^{-1}(573 \text{ K})^2}\right)\right), \tag{A.6}$$

leading to the following approximation for the energy production

$$\dot{q}'' = \Delta H_c \rho A^* exp\left(\frac{-E_a}{RT_p}\right) l_R, \tag{A.7}$$

where:

$$l_R = \frac{RT_p^2}{E_a b}. \tag{A.8}$$

Eq. A.7 corresponds to the energy production in a small part of the cotton with vertical size l_R (see figure 2.7) with constant temperature (T_p) as an approximation for the energy production in the material with vertical size l with a linear temperature gradient ($T_p - bz$).

Appendix B

Sensitivity analysis

B.1 Ignition model with temperature-dependent heat loss zone

Using the ignition model described in section 5.1.2, a sensitivit analysis on the variable T_{lim} has been performed. T_{lim} has been investigated for values 30, 40, 50, 55, 60 and 70 °C, in order to find which limiting temperature gives the best estimate for the temperature for onset of smoldering. In table B.1 the estimated temperature and deviation compared with the experimental results are shown. By taking the absolute values of the deviations for each scenario, and taking the average for each T_{lim}, 40 °C is found to give the best estimate.

B.2 Transient modeling of onset of smoldering

Using the ignition model described in section 5.1.2 and the 1D heat transfer model described in 5.2, a sensitivity analysis on the variable T_{lim} has been performed. In addition the effect on number of control volumes have been investigated. T_{lim} has been investigated for 40, 50 and 60 °C, in order to find where the limiting temperature gives the best estimate for the temperature for onset of smoldering. In table B.2 the estimated temperatures for onset of smoldering are shown. The time for onset of smoldering has also been looked at, as shown in table B.3. The results show that T_{lim} = 40 °C gives the best estimates for time and temperature. The numbers of control volumes have little effect on the temperature for onset of smoldering, but has weak affect on time.

Table B.1: Sensitivity analysis - ignition model

Density	Experimental ignition temperature	T_{lim} 30		40		50		55		60		70	
		Estimated ignition temperature	Deviation	Estimated ignition temperature	Deviation	Estimated ignition temperature	Deviation	Estimated ignition temperature	Deviation	Estimated ignition temperature	Deviation	Estimated ignition temperature	Deviation
(kg/m^3)	(°C)	(°C)	(%)	(°C)	(%)	(°C)	(%)	(°C)	(%)	(°C)	(%)	(°C)	(%)
Scenario A													
20	307	296	-2	314	1	320	2	323	3	320	2	315	1
40	318	287	-5	304	-2	321	1	327	2	325	1	320	0
60	315	290	-4	308	-1	320	1	320	1	320	1	320	1
80	309	284	-4	299	-2	313	1	316	1	321	2	333	4
100	303	302	0	320	3	338	6	346	7	344	7	339	6
Scenario D													
20	306	288	-3	295	-2	296	-2	295	-2	293	-2	291	-3
40	320	273	-8	283	-6	284	-6	285	-6	284	-6	283	-6
60	318	267	-9	274	-7	276	-7	276	-7	275	-7	274	-7
80	304	266	-7	273	-5	275	-5	276	-5	276	-5	275	-5
100	284	268	-3	275	-2	278	-1	278	-1	278	-1	276	-1
Scenario E													
20	336	286	-8	291	-7	290	-8	290	-8	289	-8	285	-8
40	302	283	-3	290	-2	289	-2	288	-2	286	-3	282	-3
60	305	273	-6	279	-4	279	-4	278	-5	277	-5	274	-5
80	300	267	-6	276	-4	278	-4	279	-4	279	-4	276	-4
100	303	266	-6	279	-4	283	-3	283	-3	283	-3	283	-3

Table B.2: Sensitivity analysis - 1D-heat transfer model combined with ignition model - Temperature at onset of smoldering

		T_{lim}		
		40	50	60
Numbers of control volume (-)	Experimental ignition temperature (°C)	Estimated ignition temperature (°C)	Estimated ignition temperature (°C)	Estimated ignition temperature (°C)
Scenario A				
100	303	312	318	318
200	303	314	318	319
300	303	315	319	319
400	303	315	318	319
Scenario D				
100	284	253	258	259
200	284	254	259	260
Scenario E				
100	303	290	291	291
200	303	290	291	291

Table B.3: Sensitivity analysis - 1D-heat transfermodel combined with ignition model - Time

		T_{lim}		
		40	50	60
Numbers of control volume (-)	Experimental ignition time (s)	Estimated ignition time (s)	Estimated ignition time (s)	Estimated ignition time (s)
Scenario A				
100	1538	1766	1872	1872
200	1538	1793	1873	1906
300	1538	1804	1898	1906
400	1538	1810	1897	1927
Scenario D				
100	15360	10438	11076	11232
200	15360	10557	11121	11276
Scenario E				
100	4740	2713	2979	2980
200	4740	2714	2966	3046

B.3 Sensitivity with different amount of water in cotton

Using the ignition model described in section 5.1.2 and the 1D-heat transfer model described in 5.2, a sensitivity analysis on the amount of water in the cotton has been performed. T_{lim} was set to 40 °C and the numbers of nodes in the calculation are 100. The sensitivity analysis in table B.4 shows that both time to and temperature at onset of smoldering are affected by the amount of water in the cotton. This is expected since to water affects both conductivity and specific heat.

Table B.4: Sensitivity analysis - Onset of smoldering with different amount of water

Water vapor weight contents	Calculated temperature for onset of smoldering	Experimental results
(%)	(°C)	(°C)
0	296	
5	312	303
10	320	
Water vapor weight contents	**Calculated time for onset of smoldering**	**Experimental results**
(%)	(s)	(s)
0	1598	
5	1776	1538
10	1962	

Bibliography

[1] Ns 3900 brannprøving: terminologi. termer og definisjoner (in norwegian). Tech. rep., Norsk Standard, 1994.

[2] Brann- og uhellsstatistikk 2006. Tech. rep., Directorate for Civil Protection and Emergency Planning, 2007.

[3] ALDUSHIN, A. P., BAYLISS, A., AND MATKOWSKY, B. J. On the transition from smoldering to flaming. *Combustion and Flame 145*, 3 (5 2006), 579–606.

[4] ALDUSHIN, A. P., BAYLISS, A., AND MATKOWSKY, B. J. On the mechanism of triggering the transition from smoldering to flaming. *Proceedings of the Combustion Institute 31*, 2 (1 2007), 2661–2668.

[5] ALDUSHIN, A. P., BAYLISS, A., AND MATKOWSKY, B. J. Is there a transition to flaming in reverse smolder waves? *Combustion and Flame 156*, 12 (12 2009), 2231–2251.

[6] ALEXOPOULOS, S., AND DRYSDALE, D. D. The transition from smoldering to flaming combustion. *Fire and Materials 13* (1988), 37–44.

[7] ANDERSON, E. E. *Thermodynamics*. PWS Pub., Boston, 1994.

[8] ANDERSON, M. K., SLEIGHT, R. T., AND TORERO, J. L. Downward smolder of polyurethane foam: Ignition signatures. *Fire Safety Journal 35*, 2 (9/1 2000), 131–147.

[9] ATREYA, A. Ignition of fires. *Philosophical Transactions of the Royal Society of London Series A-Mathematical Physical and Engineering Sciences 356*, 1748 (1998), 2787–2813.

[10] BABRAUSKAS, V. *Ignition Handbook: Principles and Applications to Fire Safety Engineering, Fire Investigation, Risk Management and Forensic Science*. Fire Science Publishers/SFPE, Issaquah, WA, 2003. pg. 302 - 304 about moisture, pg. 315 - 320 about glowing and smoldering ignition, pg. 729-730 about cotton.

[11] BABRAUSKAS, V. Ignition: A century of research and an assessment of our current status. *Journal of Fire Protection Engineering 17*, 3 (August 1 2007), 165–183.

[12] BADR, O., AND KARIM, G. A. Experimental-study of self-ignition and smoldering of moist cellulosic materials. *Journal of Energy Resources Technology-Transactions of the Asme 114*, 2 (1992), 146–151.

[13] BAR-ILAN, A., PUTZEYS, O. M., REIN, G., FERNANDEZ-PELLO, A. C., AND URBAN, D. L. Transition from forward smoldering to flaming in small polyurethane foam samples. *Proceedings of the Combustion Institute 30*, 2 (1 2005), 2295–2302.

[14] BEEVER, P. F. Initiation and propagation of smouldering reactions (ph.d thesis). Tech. rep., Department of Physical Chemistry, University of Leeds., 1986.

[15] BOONMEE, N., AND QUINTIERE, J. G. Glowing ignition of wood: The onset of surface combustion. *Proceedings of the Combustion Institute 30* (2005), 2303–2310.

[16] BOWES, P. C., AND THOMAS, P. H. Ignition and extinction phenomena accompanying oxygen-dependent self-heating of porous bodies. *Combustion and Flame 10*, 3 (1966), 221–230.

[17] BOWES, P. C., AND TOWNSHEND, S. E. Ignition of combustible dusts on hot surfaces. *British Journal of Applied Physics 13*, 3 (1962), 105–114.

[18] BROWNE, F. L. Theories of the combustion of wood and its control. Tech. Rep. 2136, USDA Forest Products Laboratory, 1958.

[19] CESTARI, L. A., WORRELL, C., AND MILKE, J. A. Advanced fire detection algorithms using data from the home smoke detector project. *Fire Safety Journal 40*, 1 (2005), 1–28.

[20] CHAN, T. K., AND NAPIER, D. H. Smouldering and ignition of cotton fibres and dust. *Fire Prevention and Technology 4* (1973), 13–23.

[21] CHAO, C. Y. H., AND WANG, J. H. Transition from smoldering to flaming combustion of horizontally oriented flexible polyurethane foam with natural convection. *Combustion and Flame 127*, 4 (2001), 2252–2264.

[22] CORRADINI, E., TEIXEIRA, E. M., PALADIN, P. D., AGNELLI, J. A., SILVA, O. R. R. F., AND MATTOSO, L. H. C. Thermal stability and degradation kinetic study of white and colored cotton fibers by thermogravimetric analysis rid c-4755-2012. *Journal of Thermal Analysis and Calorimetry 97*, 2 (AUG 2009), 415–419.

[23] DODD, A. B., LAUTENBERGER, C., AND FERNANDEZ-PELLO, C. Computational modeling of smolder combustion and spontaneous transition to flaming. *Combustion and Flame 159*, 1 (JAN 2012), 448–461.

[24] DRYSDALE, D. *An Introduction to Fire Dynamics*, 2 ed. Wiley, Chichester, 1999. pg: 261 - 289.

[25] DRYSDALE, D. *An Introduction to Fire Dynamics*, 3 ed. Wiley, Chichester, 2011. pg: 261 - 289.

[26] ECKHOFF, R. K. *Dust Explosions in the Process Industries*, 3 ed. Gulf Professional Publishing, Amsterdam, 2003.

[27] FRANK-KAMENETSKII, D. A. *Diffusion and Heat Exchange in Chemical Kinetics*. Princeton University Press, Princeton, 1955.

[28] GRATKOWSKI, M. T., DEMBSEY, N. A., AND BEYLER, C. L. Radiant smoldering ignition of plywood. *Fire Safety Journal, 41*, 6 (9 2006), 427–443.

[29] GRIFFITHS, J. F., BARNARD, J. A., AND BRADLEY, J. N. *Flame and combustion*. No. 3rd ed. Blackie, London, 1995. pg. 145.

[30] HALL, J. R. The smoking-material fire problem. Tech. rep., National Fire Protection Association - Fire Analysis and Research Division, 2012.

[31] HATAKEYAMA, T., NAKAMURA, K., AND HATAKEYAMA, H. Studies on heat-capacity of cellulose and lignin by differential scanning calorimetry. *Polymer 23*, 12 (1982), 1801–1804.

[32] HOLLEYHEAD, R. Ignition of solid materials and furniture by lighted cigarettes. a review. *Science & Justice 39*, 2 (1999), 75–102.

[33] HOLMAN, J. P. *Heat transfer*, 7th ed. McGraw-Hill, London, 1992.

[34] JONES, J. C. Thermal calculations on the ignition of a cotton bale by accidental contact with a hot particle. *Journal of Chemical Technology and Biotechnology 65*, 2 (FEB 1996), 176–178.

[35] JONES, J. C., AND WAKE, G. C. Measured activation-energies of ignition of solid materials. *Journal of Chemical Technology and Biotechnology 48*, 2 (1990), 209–216.

[36] JOSHI, K. A., RAGHAVAN, V., AND RANGWALA, A. S. An experimental study of coal dust ignition in wedge shaped hot plate configurations. *Combustion and Flame 159*, 1 (1 2012), 376–384.

[37] KANURY, A. M. *Introduction to combustion phenomena: (for fire, incineration, pollution, and energy applications)*. Gordon and Breach, New York, 1975. pg. 95-98.

[38] KELLOGG, D. S., WAYMACK, B. E., MCRAE, D. D., CHEN, P., AND DWYER, R. W. The initiation of smoldering combustion in cellulosic fabrics. *Journal of Fire Sciences 16*, 2 (1998), 90–104.

[39] KINBARA, T., ENDO, H., AND SEGA, S. Downward propagation of smoldering combustion through solid materials. *Symposium (International) on Combustion 11*, 1 (1967), 525–531.

[40] KRABBENHØFT, K. Moisture transport in wood. a study of physical-mathematical models and their numerical implementation. Tech. rep., Department of Civil Engineering, Technical University of Denmark, 2003.

[41] KRAUSE, U., AND SCHMIDT, M. Initiation of smouldering fires in combustible bulk materials by glowing nests and embedded hot bodies. *Journal of Loss Prevention in the Process Industries 10*, 4 (1997), 237–242.

[42] KRAUSE, U., AND SCHMIDT, M. Smoldering fires in bulk materials. D. Bradley, D. Drysdale, and G. Makhviladze, Eds., Center for Research in Fire and Explosion Studies, University Central Lancashire, pp. 389–400.

[43] KRAUSE, U., AND SCHMIDT, M. The influence of initial conditions on the propagation of smouldering fires in dust accumulations. *Journal of Loss Prevention in the Process Industries 14*, 6 (11 2001), 527–532.

[44] LAWSON, J. R. Environmental cycling of cellulosic thermal insulation and its influence on fire performance. Tech. Rep. NBSIR 84-2917, National Bureau of Standards (Now: National Institute of Standards and Technology), 1984.

[45] LEACH, S. V., REIN, G., ELLZEY, J. L., EZEKOYE, O. A., AND TORERO, J. L. Kinetic and fuel property effects on forward smoldering combustion. *Combustion and Flame 120*, 3 (2 2000), 346–358.

[46] LEBECKI, K., DYDUCH, Z., FIBICH, A., AND SLIZ, J. Ignition of a dust layer by a constant heat flux. *Journal of Loss Prevention in the Process Industries 16*, 4 (7 2003), 243–248.

[47] LEISCH, S. O., KAUFFMAN, C. W., AND SICHEL, M. Smoldering combustion in horizontal dust layers. *Symposium (International) on Combustion 20*, 1 (1985), 1601–1610.

[48] LOHRER, C., KRAUSE, U., AND STEINBACH, J. Self-ignition of combustible bulk materials under various ambient conditions. *Process Safety and Environmental Protection 83*, 2 (3 2005), 145–150.

[49] LUPTON, E. C., TAHLMORE, C. D., AND OBSASNIK, J. Some differences noted in the flammability of wire constructions between testing at room temperature and at elevated conductor temperatures. In *Proceedings of the 24th International Wire and Cable symposium* (Cherry Hill, NJ, USA, 1975), U. A. E. Command, Ed., U.S. Army Electronic Command, pp. 1–3.

[50] MCCARTER, R. J. Smoldering combustion of cotton and rayon. *Journal of Consumer Product Flammability 4*, 4 (1977), 346–358.

[51] MIRON, Y., AND LAZZARA, C. Hot-surface ignition temperatures of dust layers. *Fire and Materials 12*, 3 (1988), 115–126.

[52] MOUSSA, N. A., TOONG, T. Y., AND GARRIS, C. A. Mechanism of smoldering of cellulosic materials. *Symposium (International) on Combustion 16*, 1 (1977), 1447–1457.

[53] NIELD, D. A. *Convection in Porous Media*. Springer, New York, 2006.

[54] NOGAI, T., AND IHARA, M. Study on air permeability of fiber assemblies oriented unidirectionally. *Journal of the Textile Machinery Society of Japan Vol.26*, 1 (1980), 10–14.

[55] OHLEMILLER, T. J. Cellulosic insulation material. iii. effects of heat-flow geometry on smolder initiation. *Combustion Science and Technology 26*, 3-4 (1981), 89–105.

[56] OHLEMILLER, T. J. Smoldering combustion hazards of thermal insulation materials. Tech. Rep. NBSIR 81-2350, National Bureau of Standards, 1981.

[57] OHLEMILLER, T. J. Modeling of smoldering combustion propagation. *Progress in Energy and Combustion Science 11*, 4 (1985), 277–310.

[58] OHLEMILLER, T. J. Smoldering combustion. Tech. Rep. 85-3294, National Bureau of Standards, 1986.

[59] OHLEMILLER, T. J. Forced smolder propagation and the transition to flaming in cellulosic insulation. *Combustion and Flame 81*, 3-4 (9 1990), 354–365.

[60] OHLEMILLER, T. J. Smoldering combustion propagation through a permeable horizontal fuel layer. *Combustion and Flame 81*, 3-4 (9 1990), 341–353.

[61] OHLEMILLER, T. J. *Smoldering Combustion*, third ed. SFPE Handbook of Fire Protection Engineering. Society of Fire Protection Engineers, 2002, pp. 2–200–2–210. Pages 2-200.

[62] OHLEMILLER, T. J., AND LUCCA, D. A. An experimental comparison of forward and reverse smolder propagation in permeable fuel beds. *Combustion and Flame 54*, 1-3 (12 1983), 131–147.

[63] OHLEMILLER, T. J., AND ROGERS, F. E. A survey of several factors influencing smoldering combustion in flexible and rigid polymer foams. *Journal of Fire & Flammability 9*, 4 (1978), 489–509.

[64] OHLEMILLER, T. J., AND ROGERS, F. E. Cellulosic insulation material. ii. effect of additives on some smolder characteristics. *Combustion Science and Technology 24*, 3-4 (1980), 139–152.

[65] ORZEL, R. A., WOMBLE, S. E., AHMED, F., AND BRASTED, H. S. Flexible polyurethane foam - a literature-review of thermal-decomposition products and toxicity. *Journal of the American College of Toxicology 8*, 6 (1989), 1139–1175.

[66] PALMER, K. N. Smouldering combustion in dusts and fibrous materials. *Combustion and Flame 1*, 2 (6 1957), 129–154.

[67] PITTS, W. M. Nist technical note 1481: Ignition of cellulosic fuels by heated and reactive surfaces. Tech. rep., National Institute of Standards and Technology, 2007.

[68] PUTZEYS, O., BAR-ILAN, A., REIN, G., FERNANDEZ-PELLO, A. C., AND URBAN, D. L. The role of secondary char oxidation in the transition from smoldering to flaming. *Proceedings of the Combustion Institute 31*, 2 (1 2007), 2669–2676.

[69] PUTZEYS, O. M. The spontaneous and piloted transition from smoldering to flaming in polyurethane foam, 2007.

[70] PUTZEYS, O. M., FERNANDEZ-PELLO, A. C., REIN, G., AND URBAN, D. L. The piloted transition to flaming in smoldering fire retarded and non-fire retarded polyurethane foam. *Fire and Materials 32*, 8 (2008), 485–499.

[71] REIN, G. Computational model of forward and opposed smoldering combustion with improved chemical kinetics (ph.d. thesis), 2005.

[72] REIN, G. Smouldering combustion phenomena in science and technology. *International Review of Chemical Engineering 1* (2009), 3–18.

[73] RODAK, E. M., TAYLOR, R. J., HIRSCH, D. B., AND LINLEY, L. J. Effects of sample and test variables on electrical wire insulation flammability. *Journal of testing and evaluation 22*, 5 (1994), 447–450.

[74] SATO, K., AND SEGA, S. In *Fire Safety Science: Proceeding of Second International Symposium* (1989), vol. 2, International Association for Fire Safety Science, p. 87.

[75] SEMENOV, N. N. *Chemical Kinetics and Chemical Reactions*. Clarendon Press, Oxford, 1935.

[76] TAFFANEL, J., AND FLOCH, M. L. Sur la combustion des mélanges gazeux et les temperatures d'inflammation. *Comptes rendus hebdomadaires des séances de l'Académie des sciences 157* (1913), 469–472.

[77] THOMAS, P. H. On the thermal conduction equation for self-heating materials with surface cooling. *Transactions of the Faraday Society 54* (1958), 60–65.

[78] THOMAS, P. H., AND BOWES, P. C. Thermal ignition in a slab with one face at a constant high temperature, 1961.

[79] TORERO, J. L., AND FERNANDEZ-PELLO, A. C. Natural convection smolder of polyurethane foam, upward propagation. *Fire Safety Journal 24*, 1 (1995), 35–52.

[80] TRAN, H. C. *Experimental Data on Wood Materials*. Heat release in fires. E & FN Spon, London, 1995, pp. 357–372.

[81] TSE, S. D., ANTHENIEN, R. A., FERNANDEZ-PELLO, A. C., AND MIYASAKA, K. An application of ultrasonic tomographic imaging to study smoldering combustion. *Combustion and Flame 116*, 1-2 (1 1999), 120–135.

[82] TSE, S. D., FERNANDEZ-PELLO, A. C., AND MIYASAKA, K. Controlling mechanisms in the transition from smoldering to flaming of flexible polyurethane foam. *Symposium (International) on Combustion 26*, 1 (1996), 1505–1513.

[83] TYE, R. P. Heat transmission in cellulosic fiber insulation materials. *Journal of Testing and Evaluation 2*, 3 (1974), 176.

[84] WAKELYN, P. J., AND HUGHS, S. E. Evaluation of the flammability of cotton bales. *Fire and Materials 26*, 4-5 (2002), 183–189.

[85] WALTHER, D. C., ANTHENIEN, R. A., AND FERNANDEZ-PELLO, A. C. Smolder ignition of polyurethane foam: Effect of oxygen concentration. *Fire Safety Journal, 34*, 4 (6 2000), 343–359.

[86] WARNATZ, J., MAAS, U., AND DIBBLE, R. W. *Combustion: Physical and Chemical Fundamentals, Modeling and Simulation, Experiments, Pollutant Formation*, 4 ed. Springer, Berlin, 2006. pg. 142.